NOV 03 99 0830-L-02 NAS 1.29/3-2:99-09

NASA Tech Briefs

National Aeronautics and
Space Administration

Electronic Components and Circuits

Electronic Systems

Physical Sciences

Materials

Computer Programs

Mechanics

Machinery

Fabrication Technology

Mathematics and Information Sciences

Life Sciences

99-09

September 1999

2000-004118 (CFW)

INTRODUCTION

Tech Briefs are short announcements of innovations originating from research and development activities of the National Aeronautics and Space Administration. They emphasize information considered likely to be transferable across industrial, regional, or disciplinary lines and are issued to encourage commercial application.

Availability of NASA Tech Briefs and TSPs

Requests for individual Tech Briefs or for Technical Support Packages (TSPs) announced herein should be addressed to

National Technology Transfer Center
Telephone No. **(800) 678-6882** or via World Wide Web at **www2.nttc.edu/leads/**

Please reference the control numbers appearing at the end of each Tech Brief. Information on NASA's Commercial Technology Team, its documents, and services is also available at the same facility or on the World Wide Web at **www.nctn.hq.nasa.gov**.

Commercial Technology Offices and Patent Counsels are located at NASA field centers to provide technology-transfer access to industrial users. Inquiries can be made by contacting NASA field centers and program offices listed below.

NASA Field Centers and Program Offices

Ames Research Center
Carolina Blake
(650) 604-0893 or
cblake@mail.arc.nasa.gov

Dryden Flight Research Center
Lee Duke
(805) 258-3802 or
lee.duke@dfrc.nasa.gov

Goddard Space Flight Center
George Alcorn
(301) 286-5810 or
galcorn@gsfc.nasa.gov

Jet Propulsion Laboratory
Merle McKenzie
(818) 354-2577 or
merle.mckenzie@commail.jpl.nasa.gov

Johnson Space Center
Hank Davis
(281) 483-0474 or
hdavis@gp101.jsc.nasa.gov

John F. Kennedy Space Center
Gale Allen
(407) 867-6626 or
galeallen-1@ksc.nasa.gov

Langley Research Center
Dr. Joseph S. Heyman
(804) 864-6006 or
j.s.heyman@larc.nasa.gov

Glenn Research Center
Larry Viterna
(216) 433-3484 or
cto@lerc.nasa.gov

George C. Marshall Space Flight Center
Sally Little
(256) 544-4266 or
sally.little@msfc.nasa.gov

John C. Stennis Space Center
Kirk Sharp
(228) 688-1929 or
ksharp@ssc.nasa.gov

NASA Program Offices
At NASA Headquarters there are seven major program offices that develop and oversee technology projects of potential interest to industry.

Carl Ray
Small Business Innovation Research Program (SBIR) & Small Business Technology Transfer Program (STTR)
(202) 358-4652 or
cray@mail.hq.nasa.gov

Dr. Robert Norwood
Office of Aeronautics and Space Transportation Technology (Code R)
(202) 358-2320 or
rnorwood@mail.hq.nasa.gov

John Mulcahy
Office of Space Flight (Code MP)
(202) 358-1401 or
jmulcahy@mail.hq.nasa.gov

Gerald Johnson
Office of Aeronautics (Code R)
(202) 358-4711 or
g_johnson@aeromail.hq.nasa.gov

Bill Smith
Office of Space Science (Code S)
(202) 358-2473 or
wsmith@sm.ms.ossa.hq.nasa.gov

Roger Crouch
Office of Microgravity Science Applications (Code U)
(202) 358-0689 or
rcrouch@hq.nasa.gov

Granville Paules
Office of Mission to Planet Earth (Code Y)
(202) 358-0706 or
gpaules@mtpe.hq.nasa.gov

NASA TechBriefs

National Aeronautics and
Space Administration

September 1999
99-09

This document was prepared under the sponsorship of the National Aeronautics and Space Administration. Neither the United States Government nor any person acting on behalf of the United States Government assumes any liability resulting from the use of the information contained in this document, or warrants that such use will be free from privately owned rights.

BLANK PAGE

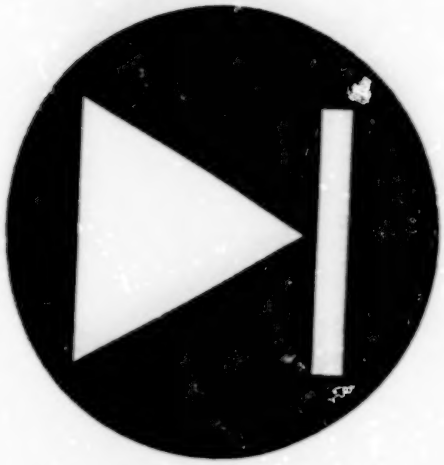

Electronic Components and Circuits

Hardware, Techniques, and Processes

BLANK PAGE

Software for Real-Time Display of Data via the Internet

This program can be used easily on almost any computer connected to the Internet.

John F. Kennedy Space Center, Florida

The JGOAL collection of computer programs facilitates the real-time display, via the Internet, of multiple streams of data from the space shuttle and its ground support equipment at Kennedy Space Center. JGOAL is also readily adaptable to other applications that involve the real-time display of real or simulated data from other sources. JGOAL is so named because it is written in the Java programming language and because the data to be displayed are first processed for distribution over the Internet by a program called "PCGOAL," which runs on a server computer that receives the data streams from a common data buffer.

JGOAL was developed to overcome a limitation of PCGOAL that previously limited the availability of the data displays to a narrow class of clients: PCGOAL packages the data in such a way as to be suitable only for display on predefined screens of client computers that run the MS-DOS operating system and that are dedicated to displaying the data. JGOAL makes it possible to display the data on almost any computer connected to the Internet.

JGOAL is written in Java to take advantage of the compatibility of Java with all major modern computer hardware and operating systems, and with popular commercially available Web-browser software. This feature reduces the time and cost of development of Internet-compatible application programs, while maintaining security and portability. Java, which is an object-oriented language, supports application-program-development constructs that enable smooth mapping from requirements to implementation; this feature shortens development time further and minimizes the effort needed for maintenance.

The major costs of implementing most client/server computing systems occur at client sites. However, this is not the case in the system based on JGOAL. Because many client computers are now equipped with Web-browser software, there is no need to configure display systems and train users of JGOAL; there are no additional client-side costs for software, configuration, maintenance, or training.

JGOAL (see figure) includes the following programs:

- The Display Translator is an application program that converts a display description (DSP) file used by PCGOAL into a Hypertext Markup Language (HTML) file and a graphical background image file. The HTML and image files are used in the placement of the data in question within a display generated by a commercial Web-browser program.
- The Display Applet program is designed to run on a client computer in a commercial Web-browser program. The Display Applet program sets up the graphical display of the JGOAL information, establishes a network connection to the Data Manager (server) application program described next, and processes the data from the network connection to the JGOAL display.
- The Data Manager application program runs on the server computer, where it receives connection requests from the Display Applet (client) program, requests data from the common data buffer (which is, essentially, another server that operates independently), and sends the requested data to the client computer.

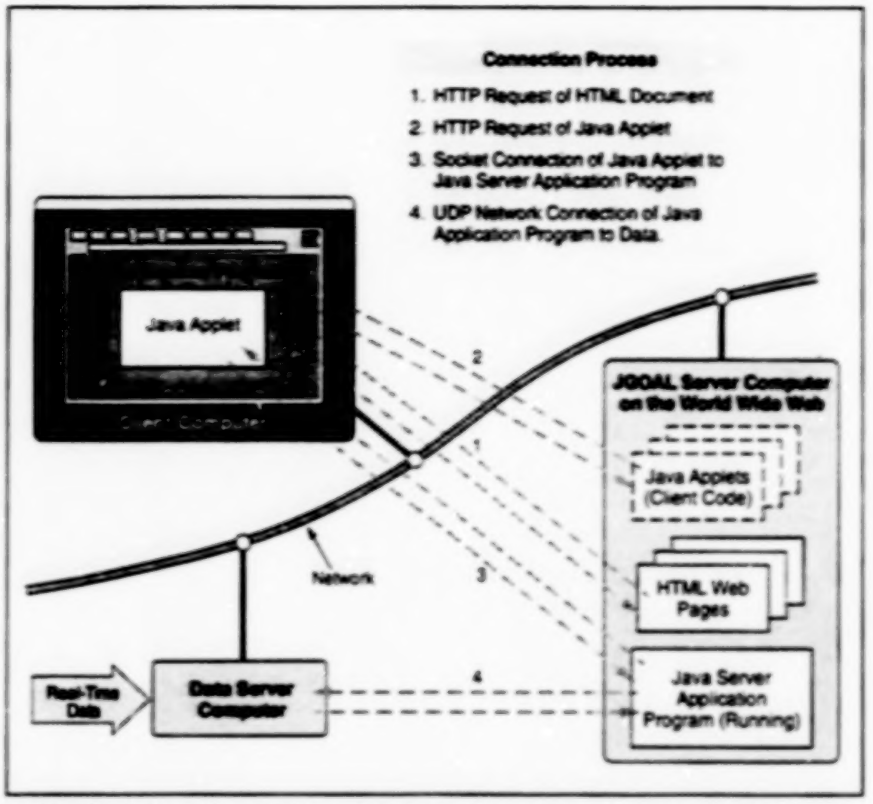

A Client Computer Is Connected to a Data Server Computer in a four-step connection process.

At the time of reporting the information for this article, the development of an upgraded combination of JGOAL and PCGOAL called "JView" was under way. JView is intended to enable a user at a desktop computer running Web-browser software to connect to a data server computer, select a data stream, and activate plot-window displays. JView is expected, when fully developed, to support the entire Kennedy Space Center user community (estimated at 800 users).

The JView application program would comprise two main subsystems: one for the server and one for the clients. The JView server subsystem would be responsible for communicating with a variety of data sources, acting as an archive of information and executable computer code, delivering requested data to clients, and regulating access through user names and passwords. The JView client subsystem would comprise JView applets (Java programs that would run within Java-enabled web-browser programs). It may become necessary to make the client programs downloadable as Java application programs.

JView client programs would support users' requests to generate selected static background displays, plot desired data streams, and manage alarm, display, and plot options. Upon startup, a JView client

program would establish a connection with a JView server and download the requested data stream along with initialization values and other pertinent auxiliary data. Once the client program was initialized and all current data were received, the client program would enter a "listen" mode, in which it would periodically receive data-change values from the server. The client could also request that the server computer gather historical data from another server computer. The client computer would periodically notify the server computer of its status and of any significant changes in its configuration.

This work was done by John M. Dockendorf, Charles H. Goodrich, Mark Long, and Steven R. Beltz formerly of I-NET, Inc.; Ryan Stansifer of Florida Institute of Technology; Kevin Gillett of Princeton University; and Will Riddle of Duke University for **Kennedy Space Center**. *Further information is contained in a TSP [see page 1].*

If your company is interested in the JView technology or need additional information, pease contact the nonexclusive license holder Netlander, Inc., Stephanie Beever, Vice President, Florida/NASA Business Incubation Center, 1311 N. Hwy US 1, Suite 129-N, Titusville, FL 32796. Telephone: (407)383-5275, fax: (407)383-5273. KSC-11949

Electronic Systems

Hardware, Techniques, and Processes

BLANK PAGE

MAP- and Laurent-AMP-Based Carrier Synchronization in GMSK

Preliminary computational simulations indicate excellent performance.

NASA's Jet Propulsion Laboratory, Pasadena, California

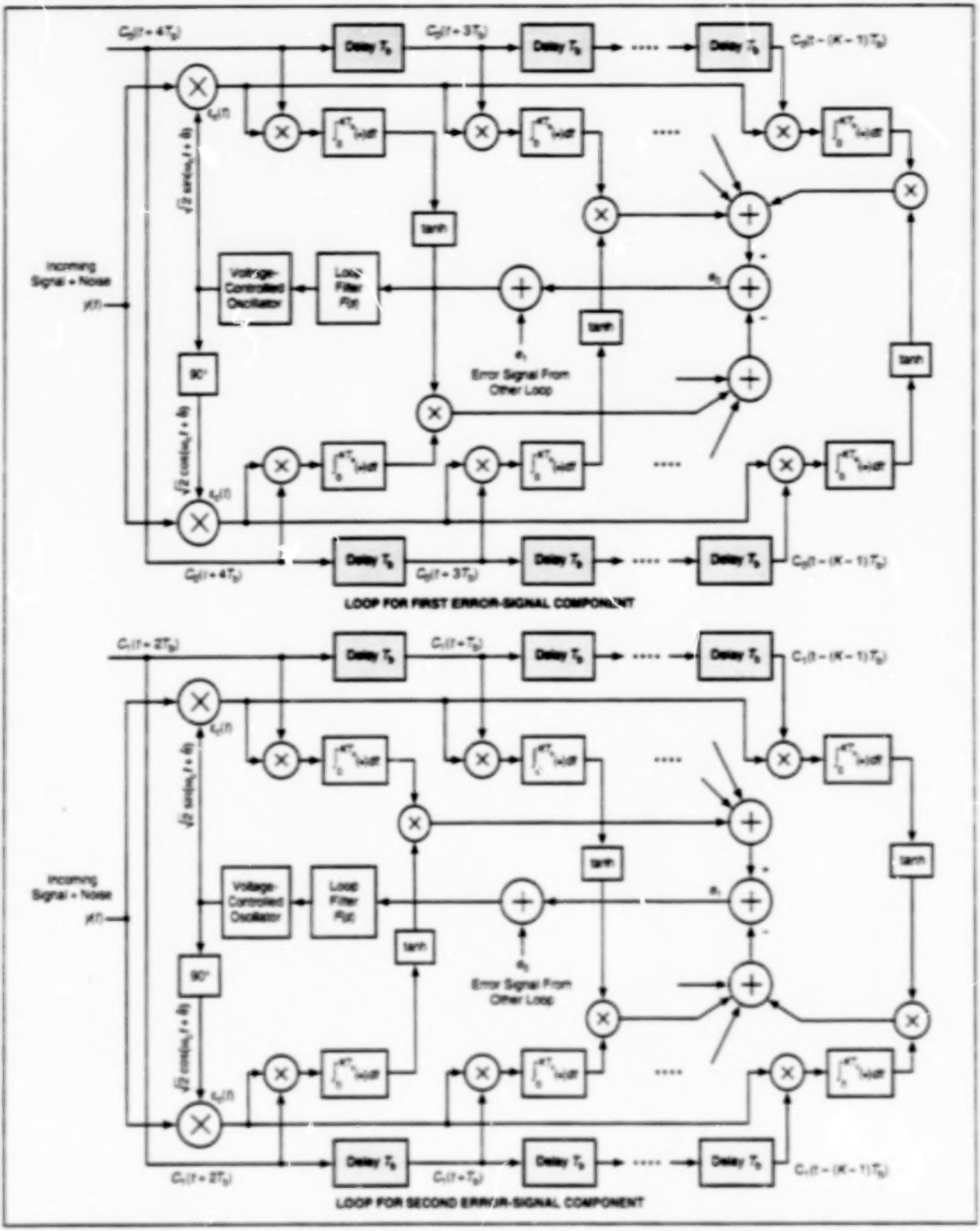

An ISI-Compensated Closed Loop for MAP estimation of the phase of a GMSK signal carrier would be constructed by superposing two loops, each corresponding to a component of a carrier-phase-error signal and to one of two pulse trains in an approximate AMP representation of the GMSK signal.

An improved method of closed-loop synchronization of a radio receiver with the phase of a carrier signal modulated by Gaussian minimum-shift keying (GMSK) has been proposed. Synchronization of the receiver with the phase of the carrier signal ("carrier synchronization" for short) is necessary for coherent detection of the data modulation. The method could improve the performances of digital wireless communication systems — particularly European cellular systems, wherein GMSK is the standard form of modulation but efficient means of carrier synchronization for coherent detection have thus far been lacking.

In GMSK, continuous-phase frequency-modulation pulses are used to convey digital data. The specific pulse shape is such that each pulse can last longer than one baud interval or bit period, T_b. The pulse duration is given by LT_b, where L is an integer that is typically chosen to equal 4. The overlapping of pulses when $L>1$ gives rise to additional inter-symbol interference (ISI) — beyond the ISI attributable to the memory associated with continuity of phase. In older GMSK carrier-synchronization methods, ISI is not taken into account; consequently, GMSK carrier-synchronization systems designed according to those methods perform suboptimally. In the proposed method, ISI is taken into account, making it possible to approach optimum performance.

The present method is based on a combination of (1) maximum *a posteriori* (MAP) estimation of digital modulation containing ISI and (2) the Laurent amplitude-modulation pulse (AMP) representation of continuous-phase modulation conveying digital data. In the Laurent AMP representation, a GMSK signal is described in terms of a superposition of 2^{L-1} amplitude-and-phase-modulated pulse streams, some containing pulses that extend beyond T_b. Thus, effects of ISI are included.

In the typical case of $L = 4$, the Laurent AMP representation contains 8 pulse trains. However, two of the pulse trains (for which the pulse durations are $5T_b$ and $3T_b$, respectively) contain most of the signal energy (the fraction of signal energy in the other six pulse trains is only 2.63×10^{-3}). Therefore, the signal can be approximated closely by the $5T_b$ and $3T_b$ pulse trains. This is advantageous because the design of a closed carrier-synchronization loop based on these two pulse trains only can be simpler than a design based on all eight pulse trains.

The loop design is derived from a combination of (1) the foregoing two-pulse-train representation and (2) an equation for an error signal as a function of the estimated carrier phase for the GMSK signal observed (along with noise) during a given number of baud intervals. The zero-error condition is an estimated carrier phase equal to the open-loop MAP phase estimate. One would close the loop by updating the phase estimate in the effort to null the error signal.

It turns out that the right side of the equation for the error signal as a function of the estimated carrier phase can be decomposed into two components, each corresponding to one of the two pulse streams in the approximate AMP representation. Thus, a closed-loop GMSK carrier synchronizer could be constructed as a superposition of two loops, each contributing one of the components of the error signal (see figure).

At the time of reporting the information for this article, the method had been tested in some computational simulations, with promising results; simulated carrier-phase synchronizers designed according to the proposed method exhibited excellent performance. Moreover, inasmuch as the second pulse stream contains significantly less energy than the first one does, it might be possible to reduce the complexity of the basic synchronizer design by use of a single-pulse-stream AMP representation of GMSK.

This work was done by Marvin K. Simon of Caltech for **NASA's Jet Propulsion Laboratory**. *Further information is contained in a TSP [see page 1].*

In accordance with Public Law 96-517, the contractor has elected to retain title to this invention. Inquiries concerning rights for its commercial use should be addressed to

Technology Reporting Office
JPL
Mail Stop 122-116
4800 Oak Grove Drive
Pasadena, CA 91109
(818) 354-2240

Refer to NPO-20482, volume and number of this NASA Tech Briefs issue, and the page number.

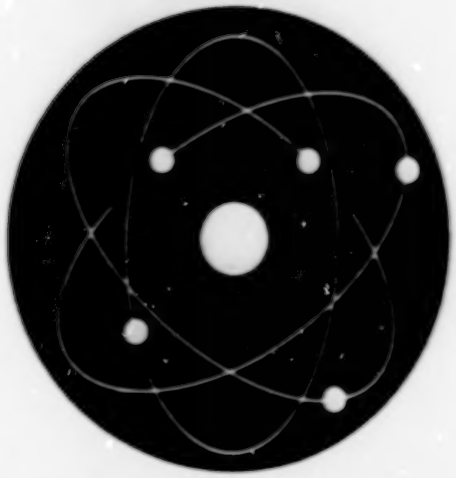

Physical Sciences

Hardware, Techniques, and Processes

Books and Reports

BLANK PAGE

Improved Array of X-Ray Microcalorimeters

Modification of array geometry increases the number of photons intercepted.

Goddard Space Flight Center, Greenbelt, Maryland

An improved array of microcalorimeters has been devised for use as photon detectors in an x-ray spectrometer for astrophysical research. The spectrometer will be used to measure the spectra of celestial objects in the "soft" x-ray range (photon energies from 200 eV to 10 keV), to a resolution much higher than has been possible until now.

Microcalorimetry is an established technique for measuring x-ray energies. Each microcalorimeter includes a small mass that absorbs incident photons. The temperature of the mass rises in proportion to the energy of each absorbed photon. The temperature rise is measured to determine the energy flux of incident photons.

Previous photon-detector designs for this instrument specified, variously, a linear or bilinear array of microcalorimeters. A linear or bilinear array is a long, narrow array that is not well matched to the circular image produced by an x-ray telescope: When the circular image is wider than the array and/or when the image is displaced widthwise, a significant number of incoming photons fail to strike the array. Inasmuch as astronomical photon fluxes are very low at the outset, any such loss of photons significantly degrades the performance of the instrument.

The improved array is a six-by-six square array in which the corner elements are not connected. In comparison with a bilinear array (see figure), it is better matched to the circular image produced by the telescope: The array is designed so that a greater fraction of incident photons is intercepted, even when the image is slightly off center in any direction.

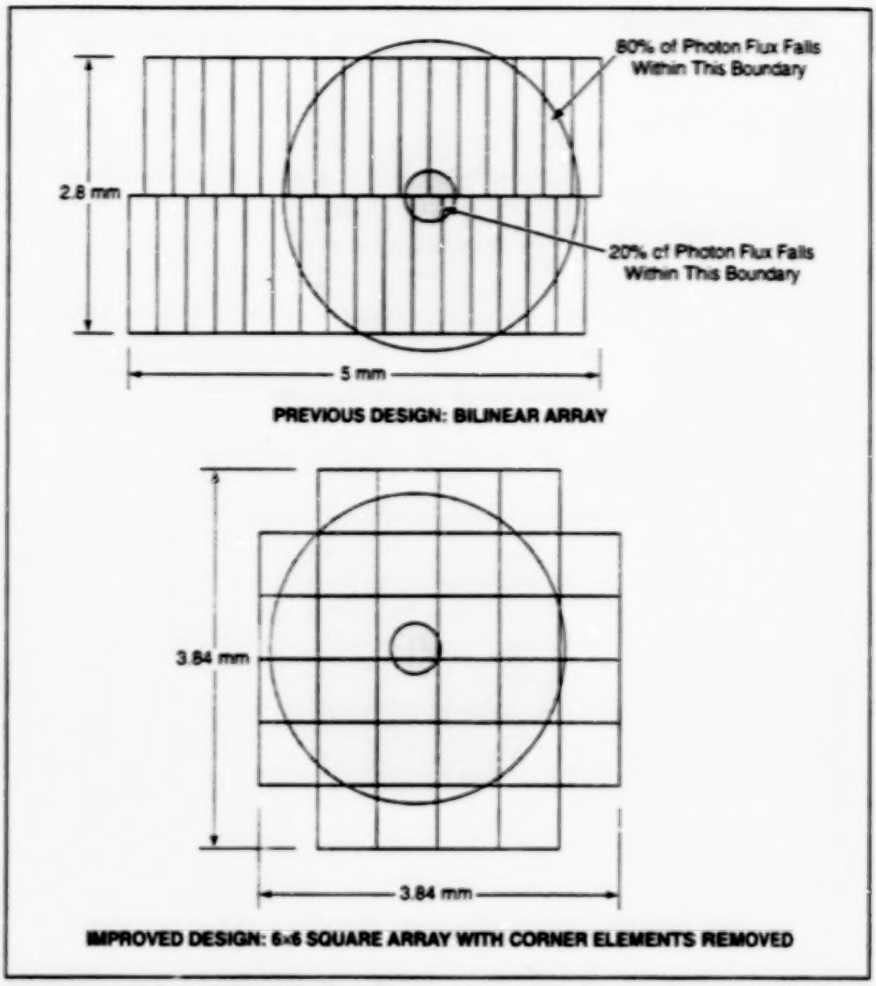

The Improved Array Intercepts More Photons (even when the circular image is slightly off center) than does the bilinear array.

This work was done by Peter Shu, Sanghamitra B. Dutta, D. Brent Mott, and Harold D. Isenberg of **Goddard Space Flight Center**. *Further information is contained in a TSP [see page 1].*
GSC-13808

Miniature Ring-Orbitron Getter Ion Vacuum Pumps

The basic orbitron configuration would be modified, shrunk, and implemented by micromachining.

NASA's Jet Propulsion Laboratory, Pasadena, California

Miniature ring-orbitron getter ion pumps have been proposed for supplying high vacuums to advanced scientific instruments expected to be developed in the next few years. Examples of such instruments include electron microscopes, ion mass spectrometers, and instruments based on electron probes.

A conventional orbitron getter ion pump (shown in the top part of the figure) includes a positively biased rod electrode on the axis of a cylindrical cavity with typical dimensions of tens of centimeters. Electrons are injected into the cavity, where they collide with and thereby ionize residual gas molecules. The resulting ions are accelerated toward, and become buried in, an ion-getter material on cavity surfaces. Because of the positively biased rod, the injected electrons get caught in orbits around the rod. The orbiting confines the electrons in a region away from the walls, thus increasing the electron path lengths and the probability that the electrons collide with the gas molecules, leading to increased efficiency of pumping.

In a conventional large orbitron getter ion pump, a negative bias is applied to the flat end walls of the cylindrical cavity to deflect the approaching electrons back into the cavity. However, the

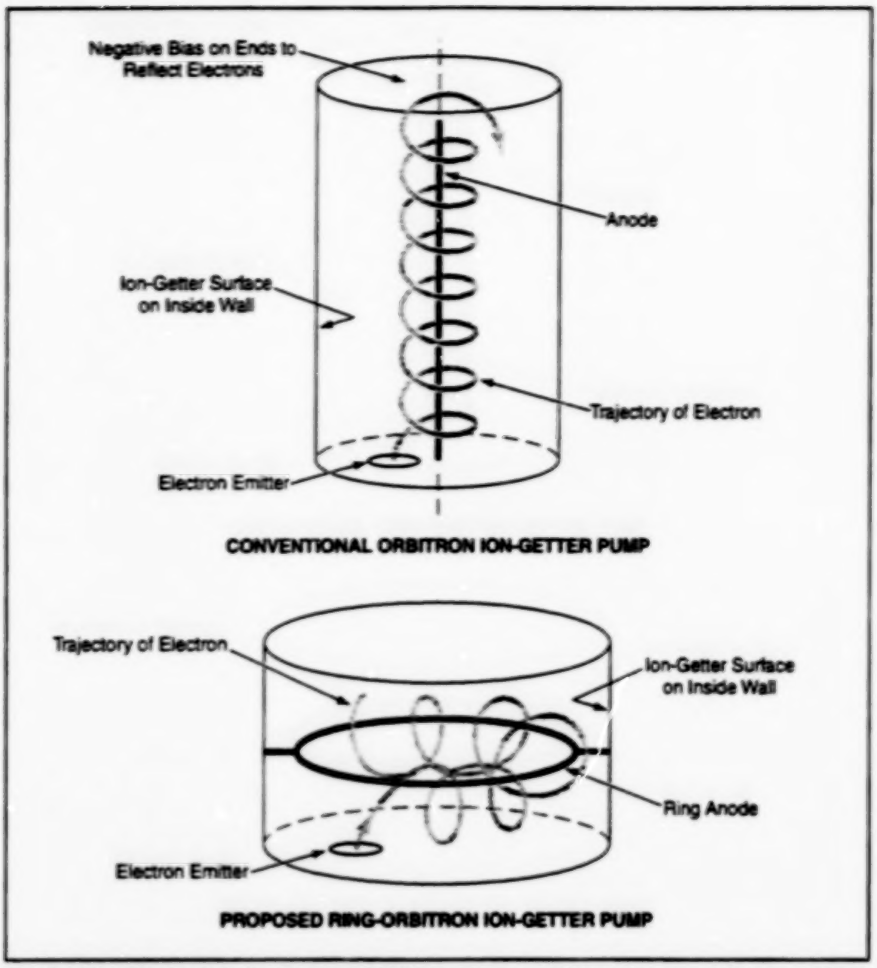

The Positive Electrode in the Proposed Orbitron Pump would be a ring around the axis, instead of an axial rod as in the conventional orbitron. In the proposed orbitron unlike in the conventional orbitron, there would be no need for negative bias on the end walls to reflect escaping electrons back into the cylindrical cavity.

required relatively large voltage becomes increasingly impractical as the size of the pump is reduced. Thus, miniaturization must entail elimination of negative bias on the end walls; this makes it necessary to find another way to confine electrons in the cavity.

The proposed ring orbitron configuration would provide the needed confinement. The rod electrode of the conventional orbitron would be replaced with a wire ring electrode, as shown in the bottom part of the figure. As in the case of the rod electrode, positive bias on the ring electrode would create a potential well, causing the electrons to spiral around the ring, and the electrons would be injected slightly off-ring to give them enough angular momentum to go into the orbits.

Unlike a conventional orbitron, a ring orbitron would be scalable to subcentimeter dimensions. In the fabrication of miniature orbitron pumps, bulk and surface micromachining and lithography could be used to define ring electrodes, ring-supporting posts, and electron emitters. Cavities could be fabricated from stacks of micromachined wafers.

This work was done by Jaroslava Z. Wilcox, Thomas George, and Jason Feldman of Caltech for **NASA's Jet Propulsion Laboratory**. *Further information is contained in a TSP [see page 1].*
NPO-20436

Digitally Tunable Color Filters and Beam Scanners

Total internal reflection would be switched on and off spatial segments.

NASA's Jet Propulsion Laboratory, Pasadena, California

Color-filtering and beam-scanning devices based on electro-optical switching of internal-reflection states have been proposed for use in display and measurement applications. Associated digital circuits would apply electronic control signals to spatial segments of these devices to obtain discontinuous spatial and/or spectral displacements of reflected and/or transmitted light beams. If this description seems a little too general, it is because the basic device concept is rather general; it could be implemented in numerous different optical and electronic configurations.

The proposed devices would take the places of the galvanometer-driven mirrors, rotating prisms, color-filter wheels, and other optomechanical devices that have been used in some beam-scanning and -filtering apparatuses until now. Unlike the optomechanical devices, the proposed devices would contain no moving parts. Relative to the optomechanical devices, the proposed devices would offer advantages of high speed and light weight.

Figure 1 illustrates a color-filter device of the type proposed, with a simple design chosen for explaining the basic principle of operation. A ferroelectric liquid crystal or other suitable electro-optical material would be sandwiched between two long Dove prisms. A continuous thin film of indium tin oxide on the sandwich contact surface of the left prism would serve as an electrode for applying an electric field to the electro-optical material. A thin film of indium tin oxide would also be applied to the sandwich contact surface of the right prism, but this film would be divided into segments to form electrodes corresponding to discrete color/beam-scanning pixels. Each electrode segment would be coated with an interference or other suitable optical filter to define the color of the pixel.

The device would be positioned and oriented so that white light entering through the lower end of the left prism would strike the sandwich contact surface at an angle slightly greater than the minimum angle for total internal reflection in the absence of applied voltage. Therefore, in the absence of applied voltage, the white light would bounce along inside the left prism through a number of total internal reflections; none of the light would be coupled to the right prism and the light would be reflected out, still white, at the top of the left prism.

If a sufficient voltage were applied between the single large electrode on the

sandwich contact surface of the left prism and one of the pixel electrodes on the sandwich contact surface of the right prism, then the index of refraction of the electro-optical material in that pixel would increase sufficiently to raise the minimum angle of incidence for total internal reflection above the actual angle of incidence. In that case, the incident light would strike the color filter in the affected pixel, so that light of one color would pass through the filter into the right prism, while the complementary color would be reflected back into the left prism. The end result would be that light of the color passed by the filter would travel along the right prism by total internal reflection and would leave the right prism at its top end, while light of the complementary color would behave similarly in the left prism and would leave that prism at its top end. If the pixels contained filters of different colors, then one could select a unique output color by applying voltage to the pixel of that color.

Figure 2 illustrates a simple non-color-discriminating beam-scanning device. This device would be similar to the device of Figure 1, except that there would be no color filters and instead of one long prism on the right side, there would be multiple small prisms — one prism for each pixel. As in the example of Figure 1, in the absence of applied voltage, light would travel along the left prism by total internal reflection and would emerge from the top of the left prism. In this case, however, the left prism would be configured so that the light emerging from the top would be traveling rightward instead of leftward. If a sufficient voltage were applied to one of the pixel electrodes, then the light would pass through to the right side and would emerge through the upper right face of the pixel for that prism. Thus, one could discontinuously scan (digitally switch) a beam of light among discrete parallel paths by applying voltage sequentially to different pixel electrodes.

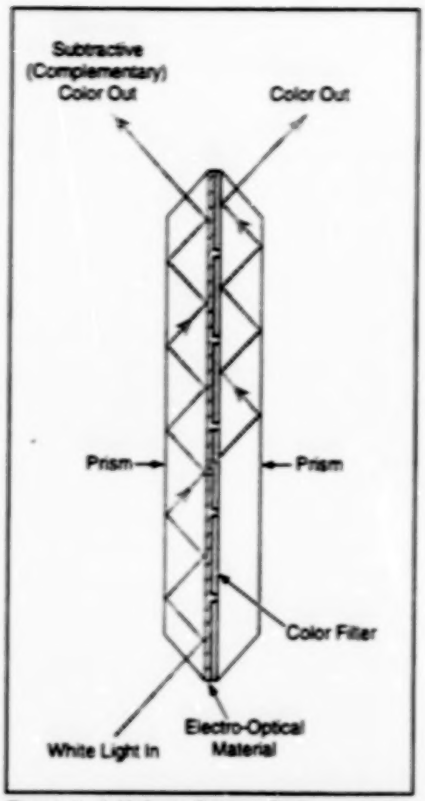

Figure 1. A Unique Output Color could be selected by applying voltage to an electrode coterminous with one of the color filters. The electric field would increase the index of refraction of the electro-optical material by an amount sufficient to stop total internal reflection at the selected filter, thereby making light pass from the left prism, through the filter, to the right prism.

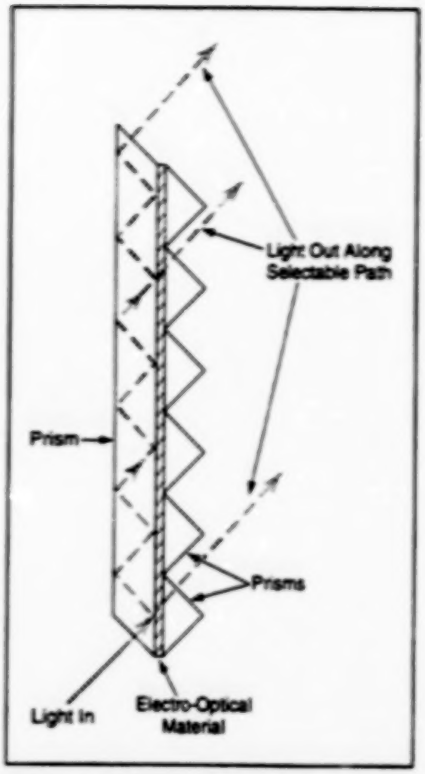

Figure 2. A Unique Output Path could be selected by applying voltage to an electrode coterminous with one of the small prisms on the right side. Except for the prism configuration and the lack of filters, this device would function similarly to that of Figure 1.

This work was done by Yu Wang of Caltech for **NASA's Jet Propulsion Laboratory**. *Further information is contained in a TSP [see page 1]*

In accordance with Public Law 96-517, the contractor has elected to retain title to this invention. Inquiries concerning rights for its commercial use should be addressed to

Technology Reporting Office
JPL
Mail Stop 122-116
4800 Oak Grove Drive
Pasadena, CA 91109
(818) 354-2240

Refer to NPO-20240 volume and number of this NASA Tech Briefs *issue, and the page number.*

Books and Reports

Lithium-Based Primary Cells for Low-Temperature Operation

A report describes an experimental study of the low-temperature electrical characteristics of commercial Li/MnO_2, Li/CF_x, Li/SO_2, Li/$SOCl_2$, and Li/BCX primary electrochemical cells. These high-energy-density cells are under consideration for use as lightweight, compact electric-power sources for scientific instruments in terrestrial polar regions and on Mars, where they could be called upon to operate at temperatures as low as –85 °C. The experiments, performed at temperatures down to –100 °C, included steady-state current-vs.-voltage measurements during discharges with various increments of load resistance from 10^5 down to 10 Ω, complete discharge tests, and ac-impedance measurements. By virtue of exhibiting the highest discharge voltages and capacities, the Li/SO_2 and Li/$SOCl_2$ emerged as the most likely candidates for use at low temperatures. Comparisons of ac-impedance data with dc current-vs.-voltage data revealed that nonohmic polarizations in the electrodes degrade cell performances more than do ohmic polarization losses in the electrolytes. Therefore, it was concluded that electrode designs should be modified to improve cell performances at low temperatures.

This work was done by Frank Deligiannis, Harvey Frank, Evan Davies, and Ratnakumar Bugga of Caltech for **NASA's Jet Propulsion Laboratory**. *To obtain a copy of the report, "Batteries for Ultra-low-Temperature Applications," see TSP's [page 1].*

NPO-20352

Evaporation of Isolated and Collections of Fluid Drops Under Supercritical Conditions

A report presents a computational study of heat and mass transfer for isolated and interacting drops of one fluid (liquid O_2) immersed in another fluid (H_2) in finite, quiescent surroundings under supercritical conditions. The mathematical models used in this study were described in three previous articles in *NASA Tech Briefs*; namely, "Model of a Drop of O_2 Surrounded by H_2 at High Pressure" (NPO-20220), "The Lewis Number Under Supercritical Conditions" (NPO-20256), and "Model of Interacting O_2 Drops Surrounded by H_2 at High Pressure" (NPO-20257), Vol. 23, No. 3 (March 1999), pages 66 through 70. The major conclusions reached in this study, which compares isolated vs. collections of fluid drops, are nearly identical to those in the cited previous articles: (1) Under supercritical conditions, the behavior of the liquid-O_2/H_2 system is one of slow diffusion. The temperature profile relaxes fastest, followed by the density profile and then by the mass-fraction profile. (2) The most important effect of clustering of drops is accumulation of oxygen in the interstitial region. As pressure increases, gradients become increasingly smeared; this behavior is qualitatively the opposite of that observed for isolated drops. (3) The effective Lewis number can be as much as 40 times the traditional Lewis number, and the spatial variations of the two Lewis numbers are different. Thus, the traditional Lewis number is not even a qualitative measure of the relative importance of heat and mass transfer. The contribution of the manuscript is the juxtaposition of the isolated vs. the collective behavior found in previous studies (see above).

This work was done by Josette Bellan and Kenneth Harstad of Caltech for **NASA's Jet Propulsion Laboratory**. *To obtain a copy of the report, "Heat and Mass Transfer for Isolated and Interacting Fluid Drops Under Supercritical Conditions," see TSP's [page 1].*

NPO-20404

Using Rayleigh Scattering To Measure Spacecraft Attitude

Two reports describe a Rayleigh-scattering attitude sensor (RSAS) — an optoelectronic instrument for determining the orientation of a spacecraft. An RSAS comprises a telescope/video-camera/image-digitizer combination that is mounted on the spacecraft and that captures images of the limb of the Earth in 355-nm-wavelength sunlight that has been Rayleigh-scattered from the atmosphere. (At 355 nm, the atmosphere scatters strongly but does not absorb significantly.) A computational model of the 355-nm radiance of the atmosphere as a function of attitude, lighting conditions, and viewing angle is then used to extract, from the image data, an estimate of the angle between the line of sight of the RSAS and the nadir. Multiple RSASs aimed along mutually orthogonal lines of sight are needed to measure attitude (or changes in attitude) with respect to more than one axis. If there are at least two RSASs and they are aimed in opposite directions along a common line, then the angle between the line and the nadir can be estimated to greater accuracy, and the attitude of the spacecraft can be estimated as well. Experiments on a prototype RSAS flown aboard the space shuttle have shown that it is possible to measure attitude angles to within ±0.05°.

This work was done by Pawan K. Bhartia and Ernest Hilsenrath of **Goddard Space Flight Center**. *To obtain copies of the reports, "Rayleigh Scattering Sensor for Spacecraft Attitude Sensing (RSAS)" and "Design Development, and Test-Flight of the Rayleigh Scattering Attitude Sensor," see TSP's [page 1].*

This invention is owned by NASA, and a patent application has been filed. Inquiries concerning nonexclusive or exclusive license for its commercial development should be addressed to the Patent Counsel, Goddard Space Flight Center [see page 1]. Refer to GSC-13858.

Diagnosing Gas-Turbine-Like Combustion by Use of PLIF

A report describes experiments in which planar laser-induced fluorescence (PLIF) of hydroxyl radicals was used to study the structures of flames in burner test rigs (a flame-tube combustor and a sector combustor) under conditions like those in combustors of aviation gas-turbine engines. Used in combustion research since the early 1980s, PLIF affords the advantage of nonintrusiveness common to optical techniques in general, plus high spatial and temporal resolution, ability to measure unstable chemical species, and potential to measure combustion temperature. Hydroxyl is often chosen for observation by PLIF in combustion research because it is a major intermediate product that plays a key role in the chemistry of combustion and because its presence in a flame zone can serve as a qualitative indication of temperature. The PLIF images from the sector-combustor experiments generally confirmed that the combustor functioned as designed. The PLIF images from the flame-tube experiments revealed previously unknown nonuniformities in flame structures; these images provided guidance for selection of an optimum number of fuel-injection points and for modifications of the fuel-injector design to improve combustion characteristics.

This work was done by Yolanda R. Hicks and Robert C. Anderson of **Glenn Research Center** *and Randy J. Locke of NYMA, Inc. To obtain a copy of the report, "Multi-Dimensional Measurements of Combustion Species in Flame Tube and Sector Gas Turbine Combustors," see TSP's [page 1].*

Inquiries concerning rights for the commercial use of this invention should be addressed to NASA Glenn Research Center, Commercial Technology Office, Attn: Tech Brief Patent Status, Mail Stop 7-3, 21000 Brookpark Road, Cleveland, Ohio 44135. Refer to LEW-16565.

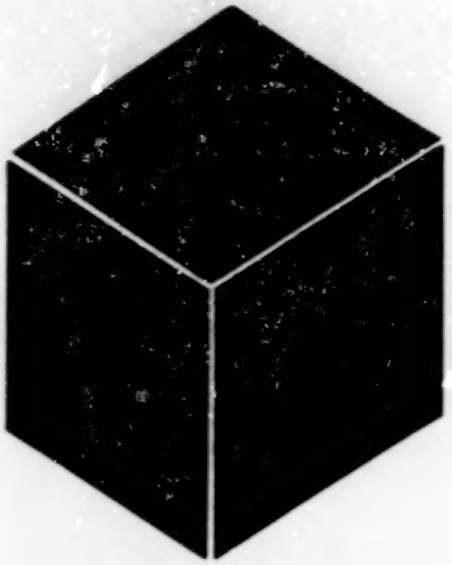

Materials

Hardware, Techniques, and Processes

BLANK PAGE

Electrodialysis To Remove Ammonium Ions From Wastewater

A simple treatment removes most of the ammonium content.

Lyndon B. Johnson Space Center, Houston, Texas

Electrodialysis has been shown to be an effective means for removing ammonium ions from wastewater without use of consumable chemicals and without adding other substances to the treated water. Provided that continuing efforts to develop efficient electrodialysis equipment prove successful, it should be possible to apply this treatment principle to wastewater streams to be recycled in life-support systems for spacecraft and other closed habitats. Effluents from some industrial processes that generate high concentration of ammonium ions may also be treatable by this principle.

In electrodialysis (see figure), an electric potential is applied across a membrane that is selectively permeable by the ions of interest — in this case, ammonium (NH_4^+). Typically, a membrane suitable for this purpose comprises a polymer matrix, within which ionophores are immobilized. Membranes based on perfluorosulfonic acid and membranes in which nonactin serves as the ionophore have been found to function efficiently as selective transporters of ammonium ions from effluent to concentrated-waste streams.

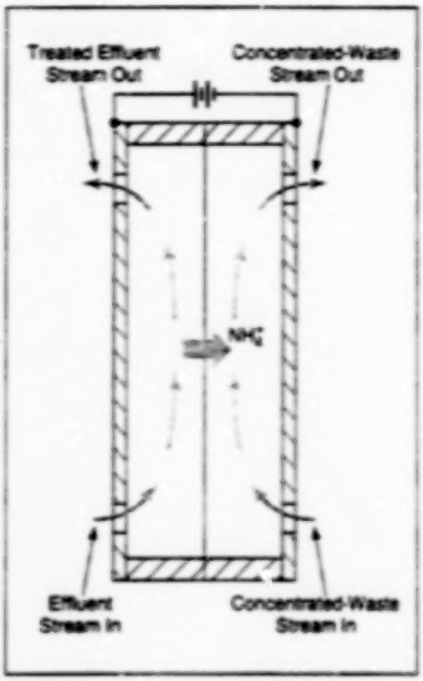

An **Electrolytic Cell** containing a suitable membrane can be used to transfer ammonium ions from one stream to another.

In an experiment, electrodialysis in an electrolytic cell containing such a membrane reduced the ammonium concentration of a simulated effluent stream from 290 to 2 parts per million. The rate of flow of the stream was 1.152 liters/day. The area of the membrane was 10 cm^2. With a potential of 10 V applied, the electric-current density in the cell was 2 mA/cm^2. With these parameters, the specific energy consumption amounted to 1.5×10^4 joules per liter of treated water. Because the minimum ammonium concentration was still above the maximum allowable (0.5 parts per million) for potability in a life-support system, further effort would be necessary to develop a practical electrodialysis unit for incorporation into such a system.

This work was done by Ella F. Spiegel of Etron Research, Inc., for **Johnson Space Center**.

MSC-22818

Analysis of Progressive Failure in Laminated Composites

The progression of damage from initial loading to final failure can be predicted.

Langley Research Center, Hampton, Virginia

A computational methodology for predicting the initiation and propagation of failures in laminated matrix/fiber composite-material structures has been developed. The methodology follows the progressive-failure approach, in which it is recognized that a laminated composite structure can develop local failures or exhibit such local damage as matrix cracks, fiber breakage, fiber/matrix debonds, and delaminations under normal operating conditions, and that such damage can contribute to the eventual failure of the structure. The ability to predict the initiation and growth of such damage is essential for predicting the performances of composite structures and developing reliable, safe designs that exploit the advantages offered by composite materials.

In this and other progressive-failure-analysis methodologies, a typical analysis involves a multistep iterative procedure in which the load on a mathematically modeled structure is increased in small steps.

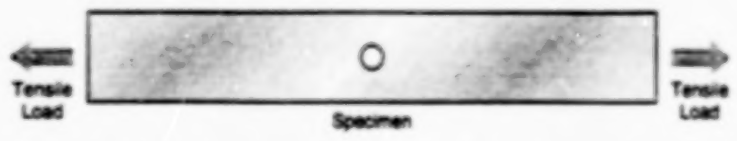

Failure Criterion	First Ply Failure Load, lb	Final Failure Load, lb	Dominant Failure Mode
Hashin's Criterion	1,550	3,212	Matrix Tension
Christensen's Criterion	1,520	3,281	Fiber/Matrix Interaction
Experimental Results	Unavailable	3,523	Unavailable

The **Final Failure Load** of a tension-loaded 20-ply laminate plate as computed by two variants of the present methodology, is compared with the experimentally determined value.

At each load step, a nonlinear analysis is performed until a converged solution (representing an equilibrium state) is obtained, assuming no changes in the mathematical submodels of the component materials of the structure. Then using the equilibrium state, the stresses within each lamina are determined from the nonlinear-analysis solution. These stresses are compared with allowable stresses for the affected materials and used to determine failure according to certain failure criteria.

If a failure criterion indicates failure of a lamina, then the mathematically modeled properties of the lamina are changed according to a mathematical submodel of degradation of the affected material properties. When this happens, the initial nonlinear solution no longer corresponds to an equilibrium state, and it becomes necessary to re-establish equilibrium, using the modified lamina properties for the failed lamina while maintaining the current load level. This iterative process of obtaining nonlinear equilibrium solutions each time a local material submodel is changed is continued until no additional lamina failures are detected. However, in this progressive failure methodology, small load step sizes were used instead of the iterative process of obtaining equilibrium solutions to minimize the effect of not establishing equilibrium at the same load level. The load step is then incremented and the foregoing analysis repeated until catastrophic failure of the structure is detected.

The present progressive-failure-analysis methodology includes the use of C^1 (slope-continuous) shell finite elements from classical lamination theory for calculation of in-plane stresses. The failure criteria used in this methodology include the maximum-strain criterion, Hashin's criterion (a stress-based criterion that predicts failures in tensile and compressive fiber and matrix modes), and Christensen's criterion (a strain-based criterion that distinguishes between fiber failures and fiber/matrix-interaction failures). The material-degradation model used in this methodology includes several options; the best option in each case depends on the choice of failure criterion and on the nature of the composite material (e.g., unidirectional composite vs. fabric composite).

The methodology is implemented by computer code that has been incorporated into the Computational Mechanics Testbed (COMET) program, which is a general-purpose finite-element analysis program. As thus augmented, COMET can predict the damage and response of a laminated composite structures from initial loading to final failure.

The methodology and its various failure criteria and material-degradation submodels were compared and assessed by performing analyses of several laminated composite structures. The results from these computations were found to be well correlated with available test data (see figure), except in structures in which interlaminar stresses are suspected of being large enough to cause certain failure mechanisms (such as debonding or delaminations) that are not modeled in this methodology.

This work was done by David W. Sleight of **Langley Research Center**. *Further information is contained in a TSP [see page 1].*
L-17660

Mixed-Carbon Anodes for Improved Li-Ion Cells

A small amount of carbon black increases retention of charge capacity.

NASA's Jet Propulsion Laboratory, Pasadena, California

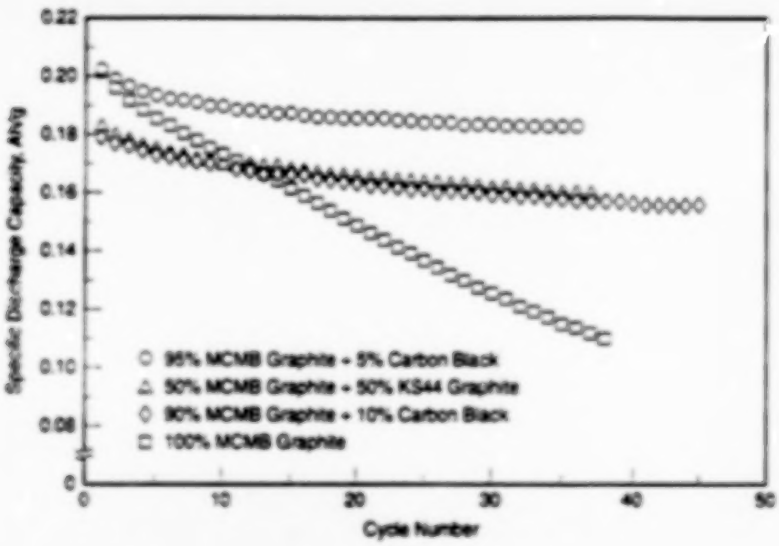

Specific Discharge Capacities of four cells were measured in cyclic charging at a current of 30 mA and discharging at a current of 60 mA.

Rechargeable lithium-ion electrochemical cells that contain anodes made from a mixture of graphite and carbon black have been found to perform better than do similar cells that contain anodes made of graphite alone. As explained in more detail below, the addition of carbon black improves performance by increasing effective electrical conductivity.

Typically, the anodes in state-of-the-art lithium-ion cells are made of amorphous carbon (coke) or graphite. Heretofore, these forms of carbon have been considered to have excellent electrical conductivity; therefore, until now, no attempt was made to incorporate carbon black or other conductive diluents into the anodes. Now, however, it has been observed that when a carbon black (more specifically, Shawanigan black) is incorporated into graphite electrodes, cycle-life performance is significantly improved.

Four lithium-ion cells were fabricated for experiments to determine the effects of incorporating carbon black into graphite anodes. In each cell, the cathode was made of $LiCoO_2$ and the electrolyte was made of a 1.0 M solution of $LiPF_6$ in a solvent that consisted of equal volume parts of ethylene carbonate (EC), diethyl carbonate (DEC), and dimethyl carbonate (DMC). The anodes of the four cells had the following compositions:

1. A commercial graphite (10-28 MCMB);
2. A mixture of 95 weight percent 10-28 MCMB and 5 weight percent carbon black;
3. A mixture of 90 weight percent 10-28 MCMB and 10 weight percent carbon black; and
4. A mixture of 50 weight percent 10-28 MCMB and 50 weight percent of another commercial graphite (KS-44).

In cyclic charge/discharge measurements, all three cells containing mixed-carbon anodes (cells 2, 3, and 4) retained greater proportions of their initial discharge capacities than did the cell containing the single-carbon anode (cell 1). Moreover, at about 15 cycles, the absolute discharge capacity of the single-carbon cell fell significantly below that of all three mixed-carbon cells (see figure).

The tentative explanation for some of these experimental results is the following:

- The carbon black particles are significantly smaller than those of 10-28 MCMB. Therefore, in the 10-28 MCMB/carbon-black electrodes, the carbon black particles are conjectured to occupy the voids between the larger 10-28 MCMB particles. In so doing, the carbon black particles increase the effective electrical conductivity of the anode by contributing to overall electrical contact among the anode particles throughout the anode.
- The 10-28 MCMB and KS-44 graphites have different particle sizes; consequently, electrical contact and electrical conductivity in the mixed-graphite anode are increased in the same manner as in the 10-28 MCMB/carbon-black electrodes.

While carbon black contributes to electrical conductivity, it also irreversibly consumes some lithium and thereby contributes to a partial irreversible loss of capacity. Apparently, the 5-weight-percent carbon black content provided sufficient electrical contact for increased retention of capacity while contributing little irreversible loss during initial charging. The anode containing 10 weight percent of carbon black exhibited approximately the same retention of capacity, but the initial irreversible loss was considerably greater than in the anode containing 5 weight percent of carbon black. From these observations, one can conclude that 5 weight percent is the optimum amount of carbon black.

This work was done by Chen-Kuo Huang and Jeffrey Sakamoto of Caltech for **NASA's Jet Propulsion Laboratory**. *Further information is contained in a TSP [see page 1].*
NPO-20603

Program Predicts Uncertainties in Properties of CMCs

This program can help engineers design reliable, long-lived structural components.

John H. Glenn Research Center, Cleveland, Ohio

Probabilistic Ceramic Matrix Composite Analyzer (PCEMCAN) is a user-friendly computer program that predicts uncertainties in the mechanical and thermal properties of ceramic-matrix composite (CMC) materials. These materials are candidates for fabrication of structural components that will be required to withstand loads at high temperatures in advanced aircraft engines. PCEMCAN is intended to help researchers develop improved CMCs for aircraft-engine components and to help engineers assess reliability and assure long operational lifetimes for those components.

PCEMCAN is an integrated computer code that embodies a combination of:

- the formal probabilistic methodology of CEMCAN [reported in "CEMCAN — Ceramic Matrix Composites Analyzer" (LEW-16327), NASA Tech Briefs, Vol. 21, No. 5 (May 1997), page 32]; and
- the fast probability integration (FPI) technique [reported in "Probabilistic Analysis of Composite-Material Structu" (LEW-16092), NASA Tech Briefs, Vol. 21, No. 2 (February 1997), page 58].

Micromechanical and macromechanical theories are implemented in CEMCAN are used to predict the strengths and other properties of CMCs. Uncertainties in primitive variables are provided as input to PCEMCAN in the form of means, standard deviations, and types of probability distributions that characterize those uncertainties. The types of probability distributions available in PCEMCAN include normal, Weibull, and log-normal.

The probabilistic integration of random primitive variables is performed by use of the FPI technique. Fewer computational simulations are needed to determine the scatter in response variables (e.g., properties of plies and laminates) when using the FPI technique than when using the Monte Carlo technique. PCEMCAN expresses the scatter in the response variables in the form of cumulative probability distribution functions (CDFs), which are useful for probabilistic analyses of structures and assessments of degrees of reliability of components. PCEMCAN also quantifies the sensitivities of the response variables to the random primitive variables.

More specifically, for given scatter of properties of fibers, properties of matrix and interphase materials, fiber volume ratio, ply thickness, and other primitive variables, the response variables (properties of the composite material) for which CDFs can be computed include the modulus of elasticity, Poisson's ratio, coefficients of thermal expansion, thermal conductivity, and laminate failure strength. PCEMCAN also computes the means, medians, and standard deviations of response variables.

These results can be used in probabilistic structural analysis to compute the reliability of a component or to asses the life of the component for a desired reliability. Sensitivity information can be used to increase reliability and to improve manufacturing processes and quality control. Finally, the probabilistic approach of PCEMCAN is beneficial in reducing the number of experiments needed, reducing (relative to the deterministic approach) the degree of conservatism in the design of a component, and making material-development and design processes more cost-effective.

This work was done by Pappu L. N. Murthy of **Glenn Research Center**, *Ashwin R. Shah of Sest, Inc., and Subodh K. Mital of the University of Toledo. Further information is contained in a TSP [see page 1].*

Inquiries concerning rights for the commercial use of this invention should be addressed to NASA Glenn Research Center, Commercial Technology Office, Attn: Steve Fedor, Mail Stop 4–8, 21000 Brookpark Road, Cleveland, Ohio 44135. Refer to LEW-16653.

BLANK PAGE

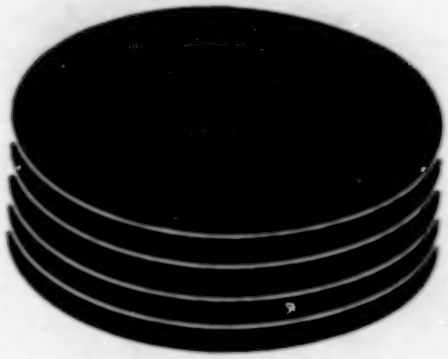

Computer Programs

Electric Components and Circuits

BLANK PAGE

Electric Components and Circuits

Program for Designing Multiple-Reflector Antenna Systems

Millimeter-Wave Optics Design Tool (MOD Tool) is a computer program for analyzing and designing multiple-reflector antenna systems that operate at microwave and millimeter wavelengths. MOD Tool is intended for use in conjunction with a computer-aided-design (CAD) program along with other specialized programs that focus, variously, on thermal, mechanical, and other aspects of design. MOD Tool is a distributed client/server application program that includes a data base of design information residing on a server computer, plus software components that perform physical-optics analyses on a variety of supercomputers. The client portion of MOD Tool includes graphical-user-interface software components that reside on a desktop computer. In addition to enabling an antenna designer to obtain computations for analysis and design of antennas, the client portion of MOD Tool serves as a data interface between (1) the antenna design and (2) the CAD and the structural and thermal designs. MOD Tool creates one standard data type for both physical optics and geometric optics and translation mechanisms for each. It can utilize parallel supercomputing to speed time-consuming physical-optics calculations. The graphical user interface relieves the antenna designer of many details, thereby simplifying the designer's task.

This program was written by Daniel Katz, Andrea Borgioli, Thomas Cwik, Chuqang Fu, William Imbriale, Vahraz Jamnejad, and Paul Springer of Caltech for **NASA's Jet Propulsion Laboratory**. *Further information is contained in a TSP [see page 1].*

NPO-20628

BLANK PAGE

Mechanics

Hardware, Techniques, and Processes

Books and Reports

BLANK PAGE

Deflection of Stretched Circular Membrane Under Pressure

Previously reported equations are generalized to account for a stretch preload.

Goddard Space Flight Center, Greenbelt, Maryland

Equations have been derived to describe the deflection of a circular membrane under both in-plane and transverse loads. More specifically, the equations describe the radial (in-plane) and perpendicular-to-the-plane deflections for the case of a circular membrane that has been stretched at its periphery with a uniform preload to keep it taut, then clamped rigidly at its periphery, and then subjected to differential pressure.

Equations for deflection of a rigidly clamped circular membrane with differential pressure but without pre-stretching were presented in "Deflection of Circular Membrane Under Differential Pressure" (GSC-13783), *NASA Tech Briefs*, Vol. 22, No. 5 (May 1998), page 78. The present equations are generalized versions of the previously reported equations. As before, the derivation follows a strain-energy/virtual deflection approach, which is common in stress-and-strain problems of this kind. The departure from the previously reported equations involves the incorporation of additional terms to account for the change in strain energy associated with work done by the preload.

The displacements of the membrane under load are described by the equations

$$w = w_0\left[1-\left(r/a\right)^2\right]^2 \quad (1)$$

and

$$u = r\left(a-r\right)\left(c_1 + c_2 r\right) + \frac{p\left(1-\nu\right)}{2\pi a E h} r, \quad (2)$$

where r is the radial coordinate, a is the radius of the clamping edge, w is the transverse displacement (that is, the deflection perpendicular to the nominal membrane plane) at radius r, w_0 is the maximum transverse displacement, u is the radial displacement at radius r, c_1 and c_2 are constants, p is the preload force, ν is Poisson's ratio of the membrane material, E is the Young's modulus of the membrane material, and h is the thickness of the membrane. The term $p(1-\nu)r/2\pi aEh$ in equation 2 describes the component of radial displacement attributable to the preload.

The radial and transverse strains are given, respectively, by

$$\varepsilon_r = \frac{du}{dr} + \frac{1}{2}\left[\frac{dw}{dr}\right]^2 \quad (3)$$

and

$$\varepsilon_t = \frac{u}{r} \quad (4)$$

The strain energy associated with stretching of the membrane is given by

$$V = \frac{\pi E h}{1-\nu^2}\int_0^a \left(\varepsilon_r^2 + \varepsilon_t^2 + 2\nu\varepsilon_r\varepsilon_t\right) r\,dr \quad (5)$$

To calculate the deflection of the membrane, one must solve the foregoing equations to find c_1, c_2, and w_0. First, one substitutes the right sides of equations (1) through (4) for the corresponding terms in equation 5. Using the resulting form of equation (5), one finds c_1 and c_2 by imposing the requirements that

$$\frac{\partial V}{\partial c_1} = 0 \quad (6)$$

and

$$\frac{\partial V}{\partial c_2} = 0 \quad (7)$$

Next, one imposes the requirement that the change in work done by the differential pressure acting through a virtual displacement equal the change in strain energy associated with the virtual displacement. If the virtual displacement is chosen to be $\delta w \propto \delta w_0$, then this requirement is expressed by the equation

$$\frac{\partial V}{\partial w_0}\delta w_0 = 2\pi q \delta w_0 \int_0^a \left[1-\left(\frac{r}{a}\right)^2\right]^2 r\,dr \quad (8)$$

where q is the differential pressure on the membrane. Eventually, one obtains the following equations:

$$\pi E h w_0^3 + 2a\alpha^3 p w_0 - \pi a^4 \alpha^3 q = 0 \quad (9)$$

where

$$\alpha^3 = \frac{6615\left(\nu^2-1\right)}{2\left(2791\nu^2 - 4250\nu - 7505\right)} \quad (10)$$

Equation 9 can readily be solved to obtain the maximum deflection, w_0, at the center of the membrane.

This work was done by Alfonso Hermida of **Goddard Space Flight Center**. *Further information is contained in a TSP [see page 1].*

GSC-14223

Making Liquid Air in Small, Economical Quantities

Liquid oxygen and liquid nitrogen are mixed on demand.

John F. Kennedy Space Center, Florida

A mixing apparatus combines liquid oxygen and liquid nitrogen to make liquid air in small, convenient quantities. Heretofore, equipment used to make liquid air by mixing was incapable of making batches smaller than 600 gallons (2,300 L). The present mixing apparatus produces liquid air on demand in batches as small as 100 liters; a batch of this size is suitable for filling self-contained breathing apparatuses like those worn by firefighters and others working in hostile environments.

It is impractical to liquefy air directly from the atmosphere because nitrogen boils at a temperature lower than that of oxygen and thus tends to evaporate faster from the liquid mixture, leaving the mixture richer in oxygen. It is therefore more practical to make liquid air by mixing the constituent oxygen and nitrogen liquids, which are readily available. Also because of the tendency toward oxygen enrichment, it is more economical to make liquid air on demand than it is to store it in large quantities that sometimes must be dumped because they become too rich in oxygen.

In the present apparatus, a tube carrying a flow of liquid oxygen converges with a tube carrying a flow of liquid nitrogen in a Y-shaped mixing device (see figure). Within this device, the tube carrying the liquid oxygen is immersed in the flow of liquid nitrogen (which is the colder of the two constituent liquids) so that the flow of liquid air receives additional cooling on its way to the collection vessel.

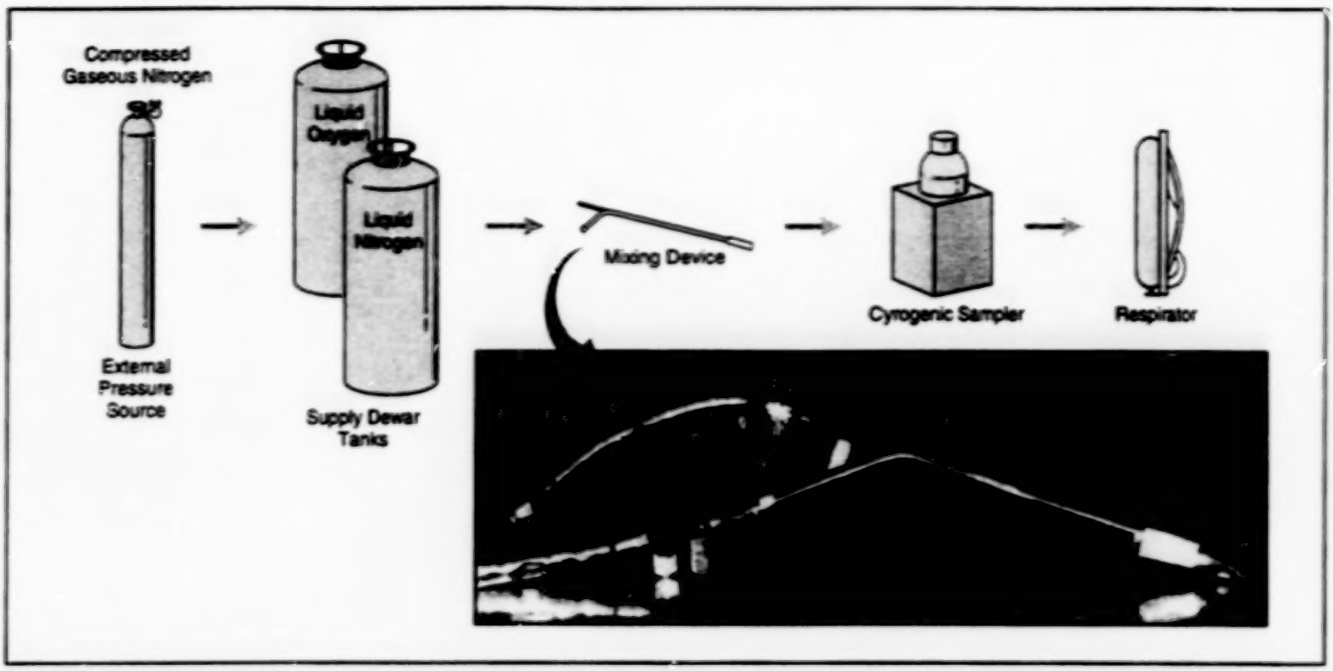

The Y-Shaped Mixing Device combines flows of liquid oxygen and nitrogen to make liquid air to supply breathing air for respirators.

Prior to mixing, the constituent liquids are stored in dewar tanks, which are pressurized by gaseous nitrogen from the liquid nitrogen supply for transfer and mixing. For safety, the pressure is limited to about 60 psi (414 kPa). The use of the same pressure for transfer of both constituent liquids helps to minimize the number of operational variables that could affect the mixing ratio. Liquid air is produced in the mixing device and collected in a receiving dewar which can then be sampled using a cryogenic sampler and used to fill respirators with no additional analysis. Sampling can also be done using the respirator as a sampler. In either method, a portable oxygen analyzer is used to determine the oxygen content.

This work was done by Robert B. Martin formerly of EG&G Florida, Inc., for **Kennedy Space Center**. *Further information is contained in a TSP [see page 1].*

This invention has been patented by NASA (U.S. Patent No. 5,678,536). Inquiries concerning nonexclusive or exclusive license for its commercial development should be addressed to the Technology Programs and Commercialization Office, Kennedy Space Center, (407) 867-6373. Refer to KSC-11774.

Accelerations of One Airplane in Wake Vortices of Another

Results of a study could guide the development of valid simplified mathematical models.

Langley Research Center, Hampton, Virginia

Accelerations of one airplane encountering a vortex or pair of vortices in the wake of another airplane were computed in a parametric study. The approach taken in the study was to systematically investigate the effects of progressively more nearly complete descriptions of the interaction of an airplane with a wake-vortex system, in order to compare the theoretical effects of some of the major simplifying assumptions that are commonly made in formulating mathematical models to represent this interaction. Despite their theoretical nature, this study and other related studies have practical significance: For example, mathematical models of airplane/vortex interaction are needed for pilot-training flight simulators. The models must represent the dominant vortex-encounter effects, yet must be simple enough to be adaptable to a variety of airplanes and simulators.

In this study, the axis of the vortices was parallel to the x axis of a Cartesian coordinate system fixed with respect to the Earth. The y and z axes were the lateral horizontal and vertical axes, respectively. In the case of a pair of vortices, the origin of the coordinate system was located between the vortices. Using a previously developed mathematical model of wake vortices, the y and z components of the vortex velocity at a given y,z location were taken to be (1) proportional to the weight and inversely proportional to the velocity and wing span of the wake-generating airplane and (2) proportional to functions of y and z that decrease with distance from the vortex cores and that include the radii and the y and z positions of the vortex cores as parameters.

In addition to the vortex coordinate system described above, there was a coordinate system fixed to the airplane body axes and five aerodynamic-surface axis systems, to model the right and left wing panels, the right and left horizontal tail panels, and the vertical tail panel. The body-axis system could be located at an arbitrary position and orientation relative to the vortex axis system. The orientation was specified by the standard airplane yaw, pitch, and roll Euler angles. The five aerodynamic-surface axis systems were placed at arbitrary positions and orientations relative to the airplane body-axis system. The equations for the wing and tail surfaces were written in general terms for planar aerodynamic surfaces with sweep, taper, and dihedral. No fuselage was modeled, and the aerodynamic surfaces were treated as originating at the center line of the airplane.

Each surface was broken up into N spanwise incremental areas. The angle of

attack and sideslip at the three-quarter-chord point of each incremental area was calculated independently of those of its neighbors. The vortex and encountering-airplane velocities were transformed into the aerodynamic-surface axis systems and used to compute aerodynamic forces, which were assumed to act at the quarter-chord point of each incremental area. The aerodynamic forces were then transformed back into the body axis system and used to compute the accelerations of the encountering airplane.

As an example case, the vortex flow field modeled in the study had the nominal characteristics of the wake of a Boeing 767 airplane, while the encountering airplane had the nominal characteristics of a Boeing 757 airplane. The majority of cases considered in this study involved roll-dominant encounters, in which the longitudinal axis of the encountering airplane was nearly parallel to the vortex *x* axis. The first case considered was that of a drag-less rectangular wing in the flow field of a single vortex. Then in a sequence of increasingly complex cases, the study progressed to the case of a complete airplane with (1) aerodynamic surfaces characterized by taper, sweep, and dihedral; (2) aerodynamic behavior that included stalling; and (3) the vortex pair in ground effect. The effects of the pitch, roll, and yaw attitudes of the airplane on the calculated accelerations were also investigated.

The numerical results of the calculations were plotted as contours of constant acceleration in a 300-by-300-ft (91-by-91-m) area centered on vortex pairs. The following conclusions were drawn from the results:

- The effects of the single vortex field extended to larger distances from the vortex core than did the effects of a counter-rotating vortex pair. However, near the cores, the effects of the vortex pair were greater and covered a larger area. In addition, the acceleration contours for the vortex pair were more complicated with more sign reversals. Thus, it appears that a vortex pair poses a potential hazard greater than that of a single vortex.
- The dominant accelerations were in roll and the *z* body axis, although significant yawing, pitching, and lateral accelerations were calculated when the vertical and horizontal tail surfaces were added to the mathematical model. Longitudinal acceleration was not a major factor.
- A nonzero lift coefficient, drag, wing dihedral, and localized stalling had negligible effects on the accelerations relative the effects of taper ratio and sweep.
- Significant distortion of all the acceleration contours occurred when the attitude of the encountering airplane was changed by 20° about any axis.
- In the case of an encounter with vortex perpendicular to the longitudinal airplane axis, the *z* and pitch accelerations were generally comparable to those for a parallel encounter, except for small areas of much larger accelerations around the vortex cores. However, the rolling, yawing, and lateral accelerations were zero because of the symmetry of the airplane.
- The effect of a ground plane at 150 ft (45.7 m) below the vortex system was minimal except when the encountering airplane was near the ground.

This work was done by Eric C. Stewart of **Langley Research Center**. *Further information is contained in a TSP [see page 1].*
L-17831

Books and Reports

Conservatism in Deterministic Structural Analysis

A paper discusses the excessive conservatism that has long been suspected to exist, because of the use of conventional (deterministic) safety factors, in the analysis and design of quasi-static structures. The origin of this conservatism is identified as a violation of statistical error-propagation laws that occurs when statistical data on loads and stresses are reduced to deterministic values and then combined through several computational processes: Because means and variations are summed to obtain tolerance limits, the embedded statistical dispersions are impelled to be summed (instead of root-sum-squared as they should be according to error-propagation laws). As a result, errors that accumulate in serial computations are larger than they should be; that is, excessively conservative. These findings are suggested to indicate a need to replace deterministic methods with probabilistic methods to prevent violations of error-propagation laws. It is also suggested that, as an alternative to adoption of fully probabilistic methods, it may be more expedient to partially convert deterministic methods to probabilistic ones to retain familiarity, confidence, and correlation with experience.

This work was done by V. Verderaime of **Marshall Space Flight Center**. *To obtain a copy of the report, "Inherent Conservatism in Deterministic Quasi-Structural Analysis," see TSP's [page 1].*
MFS-27333

Experiments on Vibration and Noise in Fuselages

A paper summarizes a continuing program of vibro-acoustic testing of two aircraft fuselage structures: (1) a 12-ft (3.7-m)-long generic aluminum test-bed cylinder that contains stiffening rings and stringers and (2) the 40-ft (12.2-m)-long fuselage of a 10-passenger turboprop airplane, made of honeycomb core and graphite/epoxy face sheets. Each structure is mounted on compliant supports that permit approximately free vibration and is instrumented with more than 200 accelerometers, which are positioned according to predictions of the first 100 vibrational modes. Excitation is provided by shakers attached to the structures at various locations. A major objective of the program is to identify natural vibration frequencies, damping rates, and mode shapes to as high a frequency as possible; the modal data will be used to validate finite-element mathematical models of vibrations and to evaluate computer codes that predict aircraft interior noise. Thus far, about 100 modes of the cylinder and 40 modes of the fuselage at frequencies below 250 Hz have been determined. Subsequent acoustic tests will focus on measurement of interior noise fields created by exterior mechanical and acoustic sources.

This work was done by Richard S. Pappa and Ralph D. Buehrle of **Langley Research Center** *and Jocelyn I. Pritchard of the Vehicle Technology Directorate of the U. S. Army Research Laboratory. To obtain a copy of the paper, "Vibro-Acoustics Modal Testing at NASA Langley Research Center," see TSP's [page 1].*
L-17851

BLANK PAGE

Machinery

Hardware, Techniques, and Processes

Books and Reports

BLANK PAGE

Software for Analyzing Performance of a Gas Turbine Engine

The user can rapidly evaluate alternative preliminary designs.

John H. Glenn Research Center, Cleveland, Ohio

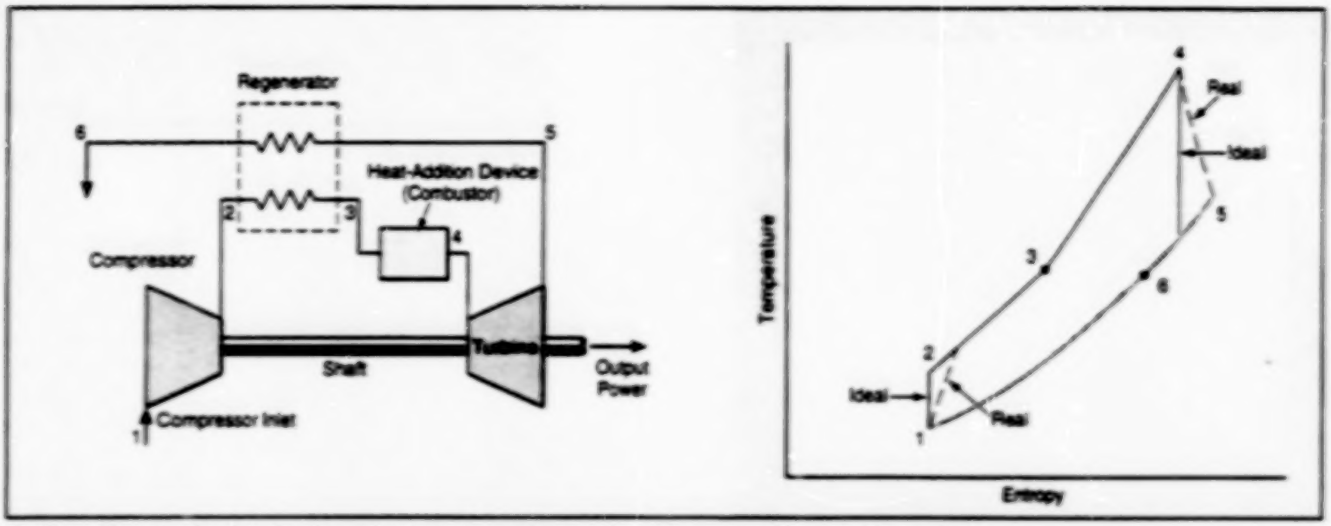

An **Open Brayton Cycle** is the theoretical basis for analysis of the performance of a gas turbine engine.

A computer program provides capabilities for numerical simulation and analysis of the thermodynamic performance of aircraft or automotive gas turbine engine. The program was developed to utilize the turboshaft-engine experience base accumulated in aerospace disciplines for designing automotive engines. Potential applications range from (1) small hybrid automotive power systems (power systems that include energy-storage subsystems) with power levels of about 25 kW to (2) heavy truck and earth-moving-machinery powerplants with megawatt power levels.

Given such inputs from the user as turbine and compressor inlet temperatures and performance characteristics of subsystems, the program calculates such powerplant thermal-performance characteristics as thermal efficiencies, specific fuel-consumption rates, cycle state points, and rates of flow of working fluids. The program also calculates data on fuel economy for a specified vehicle weight and an assumed driving cycle.

The program is based on a mathematical model of an open Brayton thermodynamic cycle (see figure). It was derived from a closed-Brayton-cycle program, "BRMAPS," developed previously for outer-space power systems energized by nuclear or concentrated solar heat sources. Written in a scientific programming language called "VSAPL," the program includes several interconnected subprograms that calculate the thermodynamic-performance quantities and that use empirical mass models to calculate the masses of essential subsystems and components. The code also computes the mass of the overall system, comprising the aforementioned components and subsystems plus interconnecting ducts and structures.

A key feature of the program is an iterative steepest-descent optimization routine that, for a given cycle temperature ratio (turbine-inlet-temperature/compressor-inlet temperature), rapidly converges to the optimum pressure ratios for maximum thermodynamic efficiency, minimum radiator area, and minimum overall system mass. Of course, performance figures can also be calculated for pressure ratios specified by the user, but by providing optimum values, the program enhances system analysis procedures drastically.

In its state of development at this writing, the program can be used to compare performances of alternative designs of automotive gas turbine engines and of hybrid systems that include gas turbine engines, under steady-state operating conditions. By use of this program, one can rapidly ascertain the payoff in fuel economy as a function of improvements in components or higher turbine inlet temperatures (made possible by use of advanced materials). Thus, the program can help to guide engine development along a most efficient and productive path. Subsequent versions of the program are expected to incorporate refinements of empirical models of component weights, plus models for volumes and costs.

This work was done by Albert J. Juhasz of **Glenn Research Center**. *Further information is contained in a TSP [see page 1].*
LEW-16709

Hybrisol Rocket Engines

These engines offer potential safety and cost advantages over solid-fuel engines.

NASA's Jet Propulsion Laboratory, Pasadena, California

"Hybrisol" denotes proposed rocket engine that would contain hybrid and solid-propellant parts within a single combustion chamber. ["Hybrid" as used here denotes a type of rocket engine in which a solid fuel is burned by use of a liquid or gaseous oxidizer and the flow of the oxidizer can be throttled to control the engine. Unlike conventional solid rocket propellants, a solid fuel for a hybrid rocket engine can be made relatively inert in the absence of the oxidizer and therefore presents little hazard of explosion or inadvertent ignition.] Inside a hybrisol rocket engine, there would be two concentric tubular energy-storage layers: an outer layer of conventional solid rocket propellant and an inner layer of solid hybrid fuel (see figure).

In operation, the solid hybrid fuel would be consumed first. As the hybrid fuel approached burnout, the burning would ignite the outer layer of solid propellant. The hybrisol concept would thus confer the following advantages:

- The use of the burning of the hybrid fuel to ignite the solid propellant would increase reliability. It would also enable a reduction in overall rocket mass because there would be no need to carry a device to ignite the solid propellant.
- The rocket would operate initially in the hybrid mode, which would afford the inherent safety of that mode plus the controllability that is typically needed during the early phase of ascent. The later burning of solid propellant would provide the high thrust typically needed in the thinner upper atmosphere.
- During ascent, mass could be reduced sharply by jettison of the empty oxidizer tank immediately after burnout of the hybrid fuel.

Detailed calculations have shown that a hybrisol design could be executed at about half the cost of its nearest competitor. In addition to the advantages mentioned above, during the hybrid phase of operation, the hybrisol concept offers the advantage of lower (in comparison with other rocket-engine concepts) pollution from its exhaust and lower temperatures. The lower temperatures make it easier to solve heat-transfer and heat-related material problems.

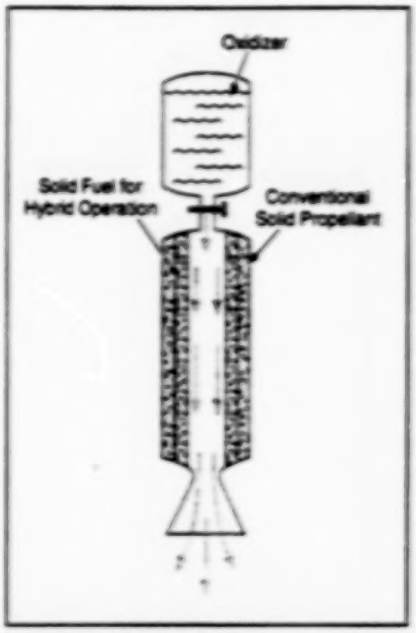

A Hybrisol Rocket Engine is a combination of a hybrid and a solid-propellant rocket engine. As the hybrid fuel nears burnout, its burning ignites the solid propellant.

Potential applications for hybrisol rocket engines range beyond the spacecraft launching market to such terrestrial applications as sounding rockets for science, distress markers, and rockets for triggering small avalanches to prevent larger ones. To the degree to which there is a toy and/or amateur rocket market, the hybrisol rockets could be attractive as safer alternatives to conventional solid-propellant rockets.

This work was done by Kumar Ramohall of Caltech for **NASA's Jet Propulsion Laboratory**. *Further information is contained in a TSP [see page 1].*
NPO-20387

Air-Purification System Utilizing Humidity Swings

This system could operate at relatively low power. *Ames Research Center, Moffett Field, California*

A regenerable, low-power air-purification system has been proposed for (1) removing toxic gases from solid-waste-incinerator exhaust and/or (2) removing trace contaminants from breathable air. The system would include a primary gas adsorber that would be regenerated in a closed-loop humidity-swing desorption cycle to ensure the destruction of contaminants before the gas stream under treatment was vented to breathable air. In comparison with a traditional thermal desorption cycle, the humidity-swing desorption cycle would consume less power. The system was conceived to be part of a life-support system in an enclosed habitat (e.g., a spacecraft or submarine); it could also be adapted to treatment of industrial and municipal incinerator exhaust streams.

The basic system concept is an outgrowth of research in which it was found that water vapor in air may suffice to displace many strongly adsorbed chemical species from a carbon-based adsorber. If humid air were circulated in reverse through a closed loop containing a saturated adsorbent column and a catalytic oxidizer, then the adsorbed contaminants should become desorbed at relatively high concentrations and be destroyed efficiently in the oxidizer. This treatment would be effected without need for high temperatures, and contaminants would be retained in the loop until destroyed.

The adsorbent column in the proposed system would contain a broad-spectrum adsorbent — possibly, though not necessarily, activated carbon, some or all of which could be platinized to provide for removal of CO and H (in addition to other gases) at ambient temperature. The catalytic oxidizer could be based on any of a number of suitable catalysts — for example, one comprised of a noble metal on alumina.

One proposed system and its modes of operation are depicted schematically in the figure. During operation in the normal mode — that is, during processing of incoming exhaust or contaminated air — all contaminants except methane and ammonia would be retained or destroyed on the platinized adsorbent in the primary adsorber. Methane could be removed in a secondary adsorber containing a hydrophobic adsorbent. Ammonia would be removed elsewhere by a condensing heat exchanger. Normal operation would be terminated when the concentration of a particular contaminant gas would rise above an allowable level.

The system would then go into a regeneration-and-oxidation mode. First, the catalytic oxidizer would be heated to its operating temperature. Three-way valves would then be turned to form the closed loop that would include a water vaporizer, the adsorbers, the catalytic oxidizer, and an acid-gas absorber. The water vapor introduced into the loop would cause the desorption of contaminant gases from the secondary and primary adsorbers. The temperature in the loop would also rise gradually, causing further desorption of contaminants less susceptible to purging by water vapor. The contaminant gases would be destroyed in the catalytic oxidizer, and any acidic oxidation products (e.g., HCl and HF) would be removed by a scrubber containing a suitable absorbent (e.g., lithium carbonate). The scrubber would not be regenerable, but it would have a long life and would seldom, if ever, have to be replaced. Upon completion of the regeneration-and-oxidation cycle, the treated air would be vented or else sent to the condensing heat exchanger for further processing.

This work was done by John E. Finn and Cory K. Finn of **Ames Research Center**, *M. Douglas LeVan of Vanderbilt University, and W. Scot Appel of the University of Virginia. Further information is contained in a TSP [see page 1].*

Inquiries concerning rights for the commercial use of this invention should be addressed to the Patent Counsel, Ames Research Center [see page 1]. Refer to ARC-14262.

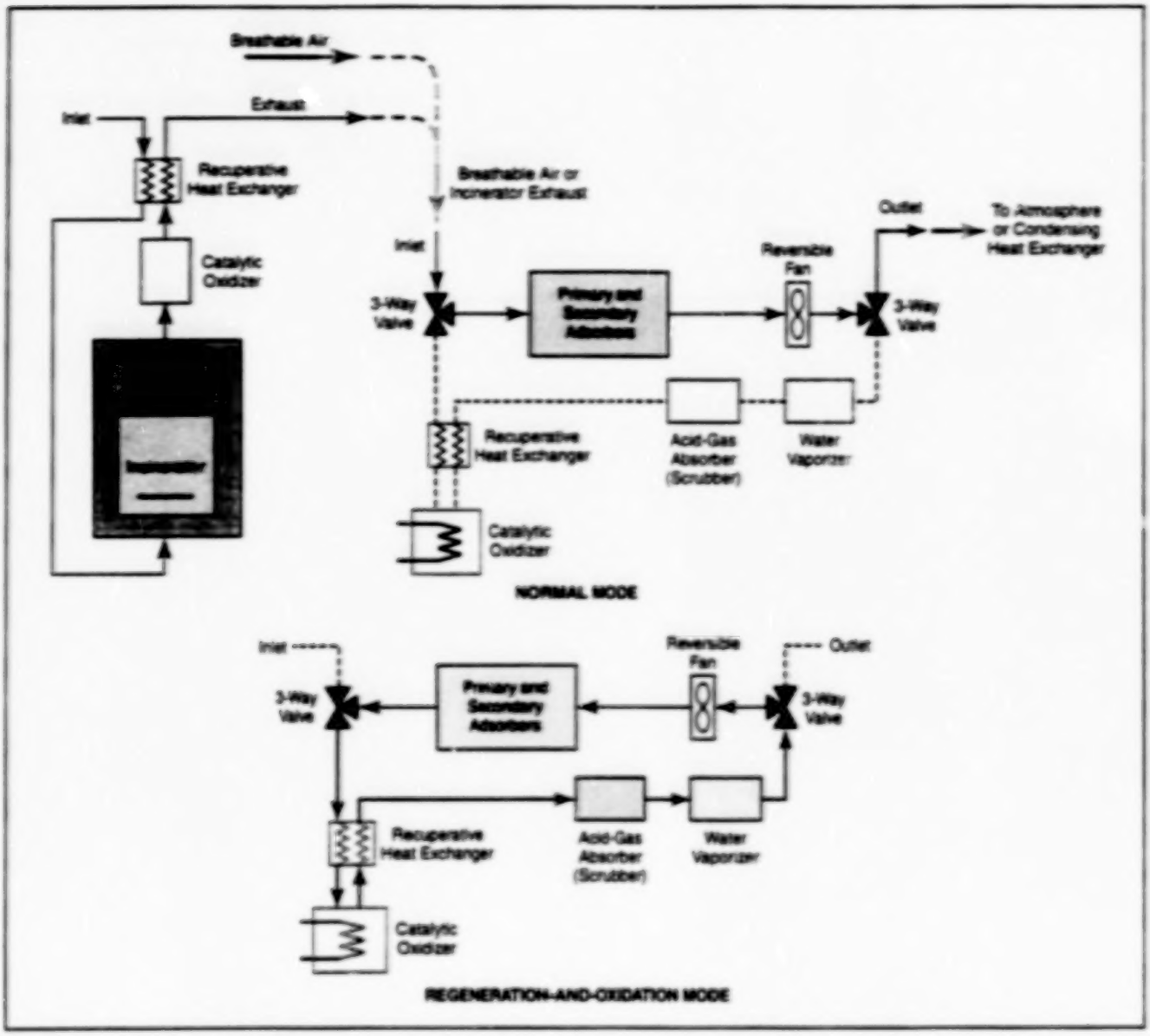

The **Proposed Air-Purification System** would operate in the normal mode to process incoming exhaust gas or contaminated air, and would then be switched into the regeneration-and-oxidation mode to regenerate the adsorbers and complete treatment.

A Precise Closed-Loop Temperature-Control System

Flow from one thermal source at a time is varied to actively control temperature.

Lyndon B. Johnson Space Center, Houston, Texas

A control system that includes a single thermal source has been designed to afford precise control of the temperature of a fluid flowing in a closed-loop system. Similar control systems could make it possible to increase production levels and to reduce risks in industrial situations in which temperatures must be strictly maintained — especially situations that involve aggressive or hazardous materials that exhibit safety-related, temperature-dependent properties. For example, in the photographic and other chemical industries, control of temperature is vital for manufacturing products and for safety of manufacturing processes; for another example, the ability to control temperature is a major concern for manufacturers of heating and cooling equipment. Overall, precise temperature-control systems like the present one can serve as valuable tools that will insure both production and safety in affected industries, in the armed services, and in the U.S. space program.

The operation of this system includes monitoring of the flow(s) of thermal (heating and/or cooling) fluid(s). Control of mass flows of thermal fluids is basic to heat-exchange systems. In traditional heating and cooling systems, constant-thermal-fluid-flow sources (e.g., pumps) and on/off valves are used to maintain temperatures at acceptable levels; this practice is expensive and is fraught with production irregularities and safety risks.

In other temperature-control systems, hot and cold fluids are constantly mixed to keep temperatures within optimum bands. In the present system, a variable flow from a single thermal source (a circulation heater or a circulation chiller, depending on whether heating or cooling is needed at the time) is used to effect precise control of the

temperature of a fluid circulating in a closed-loop system. Although the system is rated to maintain the temperature within ±1 °F (±0.6 °C) of the set point, the designer's specification predicts a range of ±0.5 °F (±0.3 °C).

The system has been installed in a space-station simulator in St. Louis, Missouri. The specification for the simulator requires that temperature be maintained within ±0.5 °F (±0.3 °C). Because the temperature tolerance for this simulator is almost as restrictive as are the temperature tolerances in other industries (including the photographic and chemical industries, heating-equipment manufacturers, and branches of the U.S. armed services), this system could also be put to good use in those industries.

This work was done by Thomas J. Poteat of McDonnell Douglas for **Johnson Space Center**. *Further information is contained in a TSP [see page 1].*
MSC-22774

Books and Reports

Gimbaled Injectors for Testing Spacecraft Thrusters

A report proposes an assembly of gimbaled valve/nozzle subassemblies for use in injecting either a propellant fluid (e.g., monomethyl hydrazine) or a propellant-simulating fluid (e.g., water) into the combustion chamber of a spacecraft thruster during hot-fire or cold testing, respectively. The proposal is a response to the problem of how to find the angle of impingement of injected fluid that results in the best thruster performance. Heretofore, tests have been conducted with injectors at various fixed angles; this manner of testing is time-consuming and does not always lead to optimum designs. The proposed gimbaled injectors would make it possible to vary the angle of impingement of the injected fluid in real time during a test, so that the impingement angle for best thruster performance could be determined more accurately and more rapidly.

This work was done by Martin Klatte of Caltech for **NASA's Jet Propulsion Laboratory**. *To obtain a copy of the report, "Gimbal Injector," see TSP's [page 1].*

This invention is owned by NASA, and a patent application has been filed. Inquiries concerning nonexclusive or exclusive license for its commercial development should be addressed to the Patent Counsel, NASA Resident Office–JPL [see page 1]. Refer to NPO-20520.

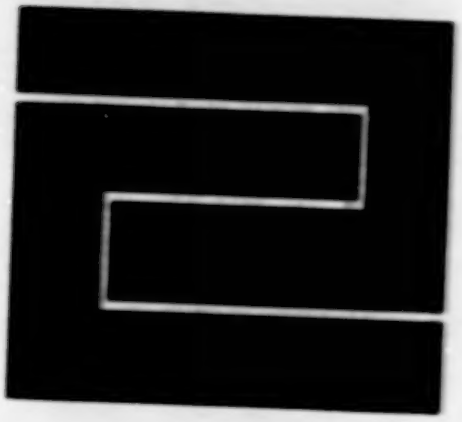

Fabrication Technology

Hardware, Techniques, and Processes

BLANK PAGE

Adaptable Drill Guide

This tool is easy to use and gives accurate, repeatable results.

Ames Research Center, Moffett Field, California

The tool shown in the figure is a drill guide that can adapt to a curved or flat surface. The main function of the adaptable drill guide is to keep the axis of a drill perpendicular to the surface at the location of the hole to be drilled. The tool can also be used to guide a reamer into a drilled hole, to control the depth of drilling or reaming, and to guide tools other than drills and reamers. With simple changes in dimensions, the basic design of the tool can readily be adapted to drill bits and reamers of various diameters.

A vacuum pump and connecting hose are needed to operate the tool. The tool includes suction-cup feet; it is attached to the surface of a workpiece by applying vacuum to the suction cups. In this way, it can even be attached to a lubricated surface without need to remove the lubricant.

Other aspects of the design and use of the tool are best described in terms of the following typical sequence of operations:

1. A pointer is inserted in the drill guide, extending past the suction cups.
2. The drill guide is maneuvered to place the pointer at a desired marked location (e.g., the center of a hole to be drilled) on the workpiece.
3. With the pointer pressed gently on the surface at the desired location, the drill guide is moved to bring the suction cups into gentle contact with the surface.
4. Vacuum is applied, causing the suction cups to pull the drill guide toward the workpiece surface until tooling balls mounted inside the suction cups make contact with the surface, providing a stable drill-guide base.
5. The pointer is removed from the drill guide.
6. A drill, reamer or other tool bit, mounted in a modified holder attached to a conventional hand tool, if necessary, is inserted in the drill guide.

Prior to the development of this tool, it was necessary to either rely on a skilled technician or else use a complex, computer-controlled five-axis milling machine to make a hole perpendicular to an arbitrary surface at an arbitrary location. In the case of a skilled technician, the degree of accuracy and repeatability of the hole is open to question. In contrast, this tool makes it possible to locate and orient drilled holes accurately and repeatably, without need for expensive machinery like a five-axis milling machine.

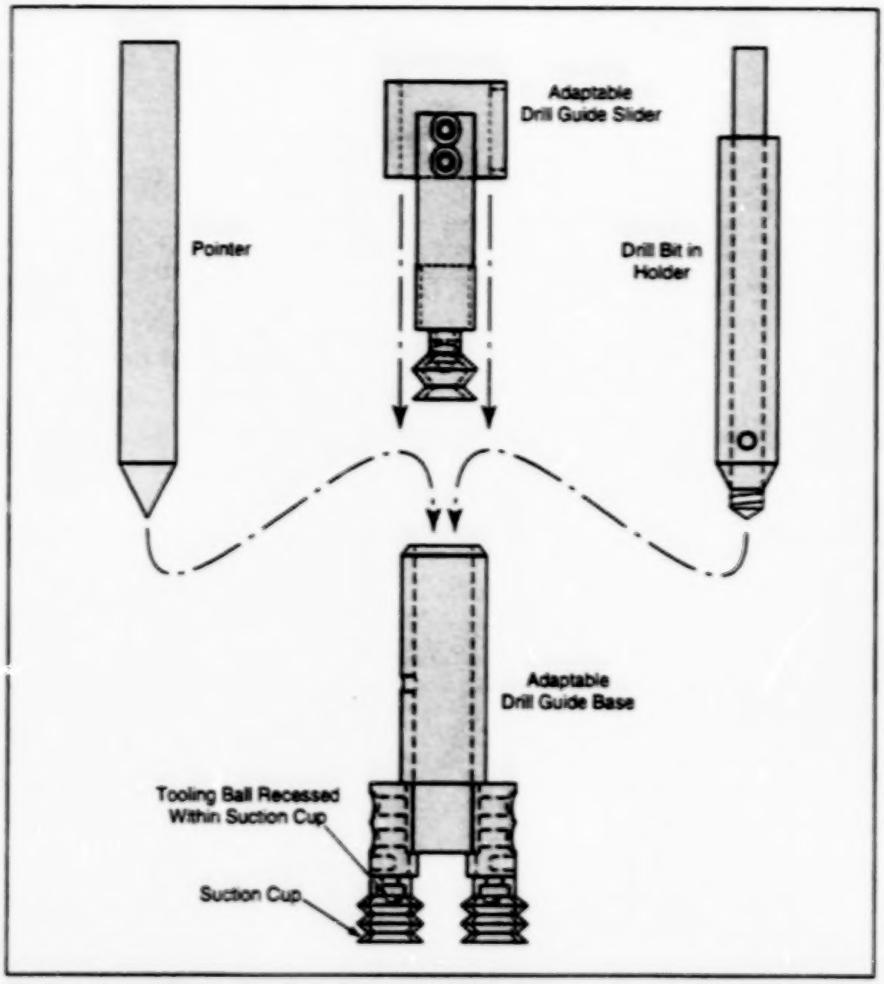

Suction Cups With Tooling Balls Recessed Within Them provide attachment and a stable geometric reference for the drill guide.

This work was done by Earl T. Daley and Lawrence W. Whiteside of **Ames Research Center**. *Further information is contained in a TSP [see page 1].*

Inquiries concerning rights for the commercial use of this invention should be addressed to the Patent Counsel, Ames Research Center [see page 1]. Refer to ARC-14259.

Mathematics and Information Sciences

Hardware, Techniques, and Processes

Books and Reports

BLANK PAGE

BLANK PAGE

Characterizing Nonlinear Dynamics by Use of Wavelet Analysis

Wavelets can be used to determine the degree and type of nonlinearity.

Dryden Flight Research Center, Edwards, California

A method to detect and to characterize the type of nonlinear dynamics in an aeroelastic system involves the utilization of information from wavelet processing of measurement data. This method is intended to assist in identifying unmodeled dynamics of aircraft during flight testing.

Some background information is prerequisite to an explanation of this development. The term "wavelet" as used here denotes a signal that is nonzero for a short time. The relevant wavelet in the present case is the Morlet wavelet, which is essentially a windowed sinusoidal signal of finite length. The Morlet wavelet is a function of parameters, called "scale" and "position", that affect, respectively, the period of the sinusoidal component and the time when the nonzero component is centered. Wavelet processing involves computation of the magnitudes of correlation between a measured signal and wavelets of different scales and positions. The wavelets with the highest correlation magnitudes represent dominant features in the measurement data.

Wavelet analysis inherently extracts time-varying features of a signal because of the short duration of the nonzero portion of the wavelet. The wavelets at a position in time determine only the features of the signal near that position. Thus, the changes in wavelets that correlate highly with the signal at different times indicate the changes in features of the signal as time progresses.

In the present method, responses from several configurations of an aeroelastic test bed are analyzed to determine the nature of the nonlinear dynamics that affect an aeroelastic system. The various configurations include various springs associated with pitch movement of a wing assembly. The forces generated by these springs can vary linearly with pitch angle or can vary nonlinearly, as in the cases of hardening or softening springs. Pitch angles are measured during free decay of oscillations of the system in response to an initial pitch placement.

The figure presents maps that result from wavelet processing of pitch responses for different system configurations. These maps can be regarded as three-dimensional in the sense that they depict magnitudes of correlation as functions of wavelet scales and positions. The color at each point in a map indicates the magnitude of correlation; specifically, white represents low correla-

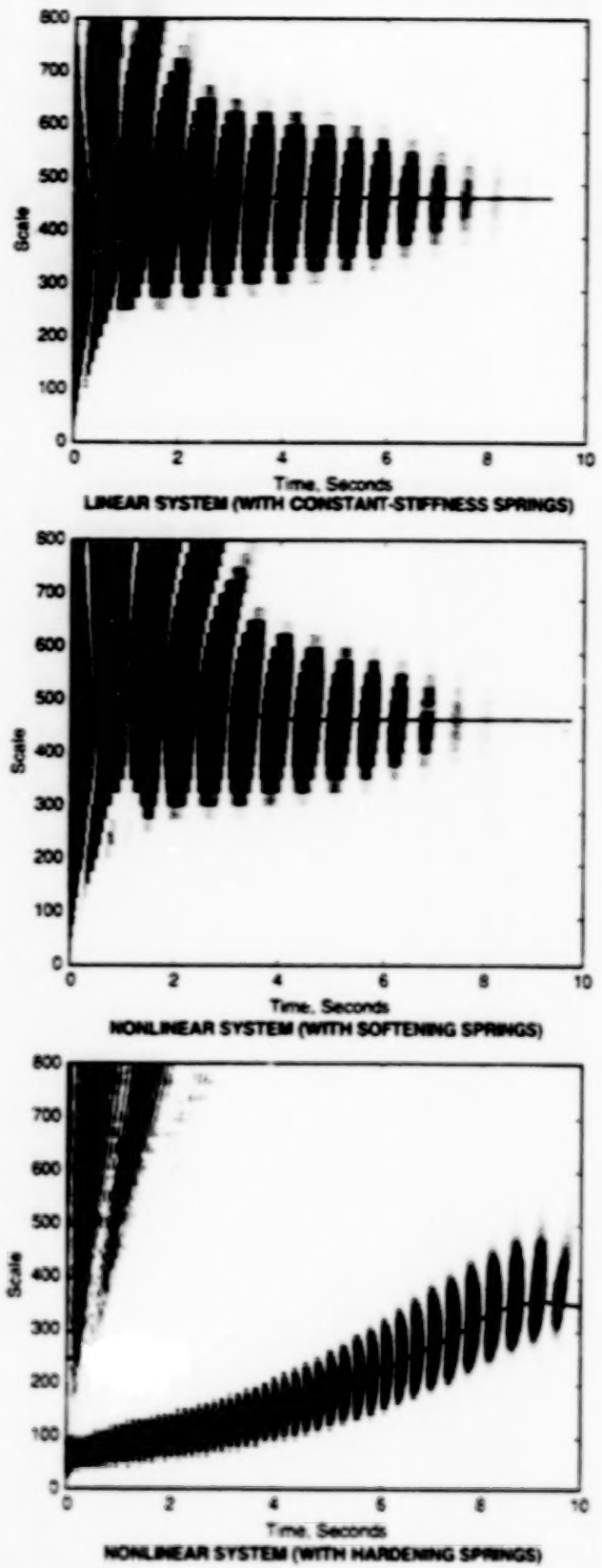

These **Maps Were Generated by Wavelet Analysis** of linear and nonlinear pitch responses of an aeroelastic system in a test bed with three different types of springs.

tion, the color changes gradually to darker levels of gray as the correlation increases, and the color becomes blue for particularly high correlation.

The dominant features of each map are extracted by identifying correlation peaks. Because these peaks are sometimes difficult to identify visually from the colored two-dimensional representations of the three-dimensional maps, a curve is drawn in each map to indicate the scale associated with the dominant feature at each position in time.

The dominant features extracted from the wavelet maps clearly indicate the presence of a nonlinearity in the aeroelastic dynamics. The curve is level and shows no change in scale for the dominant feature of the response from a linear system, but the curves vary, showing changes in scale for the dominant features of the responses from the nonlinear systems. This result is expected because (a) the response from a linear system should be a decaying sinusoid that has a constant frequency, while (b) the response from a nonlinear system should be a decaying sinusoid with a changing frequency. Thus, it is straightforward to detect the presence of nonlinearity from the variation in scale shown by the curve through the correlation peaks in a map.

The type of nonlinearity can be characterized by the type of change in the curve. The response from a hardening spring features a decreasing frequency, so its map should show an increasing scale. Conversely, the response from a softening spring features an increasing frequency, so its map should show a decreasing scale. The curves indicate these behaviors, demonstrating that wavelet analysis provides means for both detection and characterization of nonlinear dynamics.

This work was done by Rick Lind and Martin Brenner of **Dryden Flight Research Center** *and Kyle Snyder of the University of Tennessee Space Institute. Further information is contained in a TSP [see page 1].*

DRC-98-42

Program for Designing a Mechanical System

This program offers advantages of ease of use, accuracy, efficiency, and speed.

John H. Glenn Research Center, Cleveland, Ohio

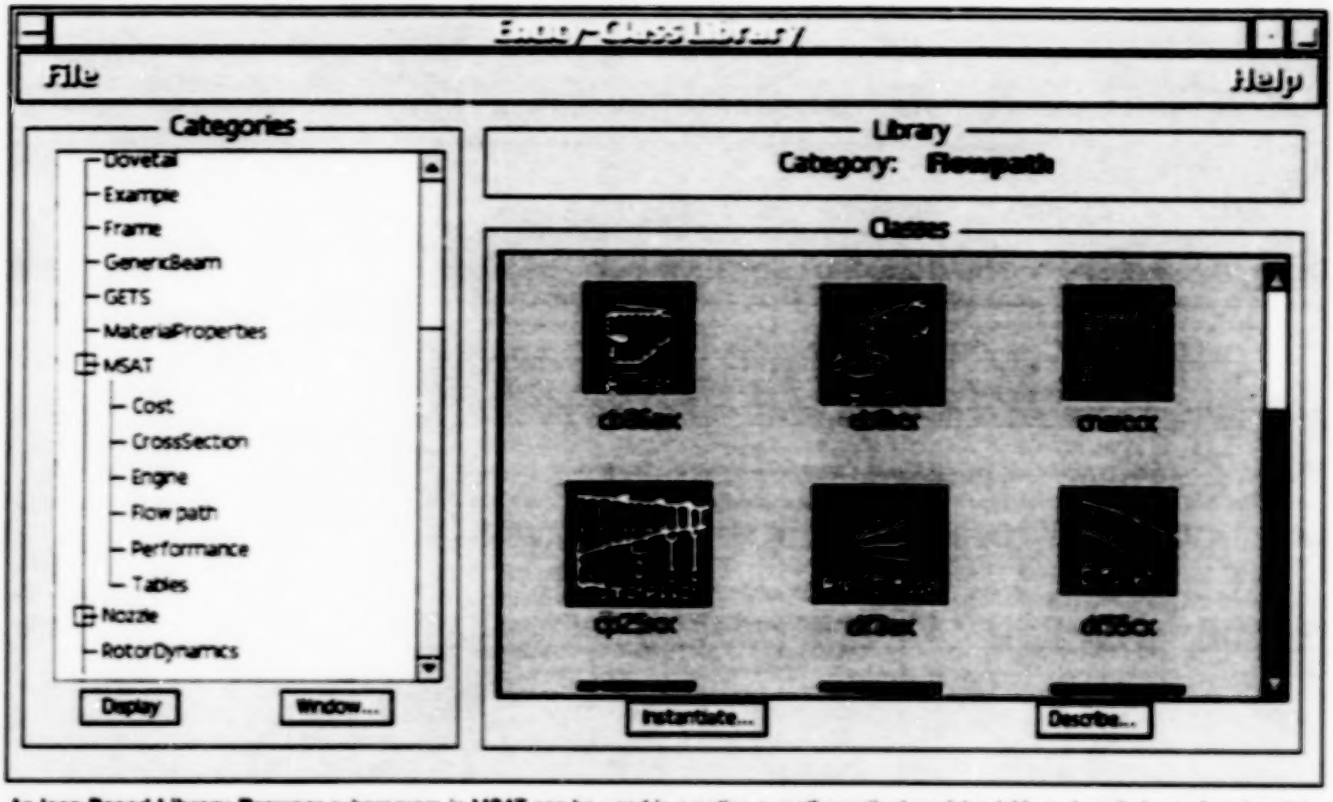

An Icon-Based Library-Browser subprogram in MSAT can be used in creating a mathematical model quickly and easily by performing pick-and-drop operations on the relevant icon(s). Here the icons represent components of an aircraft turbine engine.

Mechanical System Design/Analysis Tool (MSAT) is a user-friendly software system that facilitates and accelerates the processes of synthesizing and analyzing designs of mechanical systems. MSAT is particularly well suited for designing aircraft engines. MSAT can be used in the preliminary-design stage as well as in the detailed-design stage of a product-development process.

MSAT is a multicomponent, multidisciplinary program with a modular architecture that organizes design-analysis tasks around object-oriented representations of (1) components of the engine or other system that one seeks to design, (2) analysis programs, and (3) data-transfer links among the constructs listed in (1) and (2). The modular architecture enables the rapid generation of input data streams for trade-off studies of various configurations of the system to be designed. Once the user has set up a sequence of computations, the data-

transfer links automatically transport output from one analysis/design program for use as input in the next analysis/design program in the sequence. The computations are managed via constraint propagation — that is, by reference to constraints provided by the user as part of the design definition.

MSAT provides a global perspective on system design. Building from subcomponents and components, the user sets detailed requirements for performances of components and of the system to be designed. The plug-and-play software framework of MSAT enables the user to add new analysis/design programs and/or components of the system to be designed and to perform trade-off studies rapidly; this capability helps to increase the quality of the ultimate design.

The plug-and-play feature of MSAT can also be utilized to make MSAT itself more versatile: New optimization and robust design software modules can be plugged in without extensive effort. As advanced computer programs are developed, the user can plug them in quickly, without having to delete older programs. This building-block application to the extension and improvement of MSAT is expected to reduce both the cost of further development of MSAT itself and cost of designing engineering systems by use of MSAT.

MSAT offers advantages of accuracy, efficiency, and speed. MSAT promotes accuracy by detecting errors in data entered by the user. A mathematical model of an engineering system can be built quickly and easily (see figure), and once the model has been built, the user does not have to rebuild the model for subsequent analysis. MSAT manages an optimization program and other analysis/design programs in performing multiple iterations without interaction with the user. In a typical case in which five iterations would be needed to arrive at a reasonable product design by conventional means, MSAT can perform the same analysis in one run, thereby saving about 80 percent in time and cost.

MSAT is expected to be integrated with NASA's Numerical Propulsion System Simulation (NPSS) computer program, which is used for coupling computer codes for the design and analysis of propulsion and propulsion/airframe systems.

MSAT has already been integrated with Monte Carlo, design-of-experiments, response-surfaces, and optimization software modules to provide a capability for robust preliminary design and uncertainty analysis. This capability can be exploited to determine whether a product is underdesigned (poses an excessive risk) or overdesigned (costs more than necessary).

This work was done by Charles Lawrence of **Glenn Research Center** *and HuaHua Lee, Mark Kolb, and Jack Madelone of General Electric Co. Further information is contained in a TSP [see page 1].*
LEW-16710

Automation Language for Managing Operations

This software provides a facility for capturing expertise and procedure.

NASA's Jet Propulsion Laboratory, Pasadena, California

Automation Language for Managing Operations (ALMO) is a computer program that assists a human operator at a central control station in monitoring and controlling a complex equipment system that includes multiple subsystems connected in a digital communication network. Still undergoing development, ALMO is designed specifically for automating the operations of NASA's Deep Space Network (DSN). ALMO could be modified for use as control software in other applications that involve monitoring and control; examples include assembly lines, chemical-processing plants, and environmental management systems.

ALMO assists in the automation of operations by providing a facility for expressing procedure and operators' knowledge in the form of instructions executed by software. These instructions interact with the subsystems via a transport layer.

ALMO comprises two main components: the ALMO language and the ALMO engine/interpreter. The ALMO language is an interpreted programming language that is used to write blocks in the control software of the DSN. As used here, "block" denotes a software construct equivalent to a subroutine that performs a specific function. A block contains preconditions, one or more directive(s) to subsystems, and post-conditions. A block is executed either from a command line or from a graphical user interface for a subprogram associated with a temporal-dependency network (TDN), which is a directed graph of interconnected nodes that represents an end-to-end sequence of operations. The TDN subprogram is equivalent to a main program that calls a subroutine at the appropriate time.

ALMO contributes to automation in several ways:

- It provides visibility for information about subsystems.
- It affords an extensive facility for executing logistics involved in system operations.
- The ALMO language can be characterized as a scripting language that can represent most, if not all of a human operator's actions in operation of a subsystem. ALMO retrieves monitor data and event messages and enables a block to react to them. In this respect, ALMO reduces the operator's workload, enabling the operator to monitor and control multiple subsystems, and thereby reduces the cost of operation.
- ALMO provides means to detect anomalies via subsystem monitor data, event messages, and directive responses, and alerts the operator when it detects an anomaly.
- ALMO reinforces the concept of modular programming, in that blocks are written as modules. Modules can be reused for different subsystems and in different applications; the number of blocks that must be written for a given application is thus smaller than it would otherwise have to be; the cost of maintaining the software is also correspondingly lower.
- ALMO can be used as a means for knowledge engineering and acquisition of knowledge.

This work was done by Paul Pechkam and Patricia Santos of Caltech for **NASA's Jet Propulsion Laboratory**. *Further information is contained in a TSP [see page 1].*
NPO-20587

Image Smoothing and Edge Detection Guided by Stereoscopy

Edges can be detected with comparable performance at various distances.

NASA's Jet Propulsion Laboratory, Pasadena, California

Original Image

Edges Detected at $\sigma = 1$

Edges Detected at $\sigma = 2$

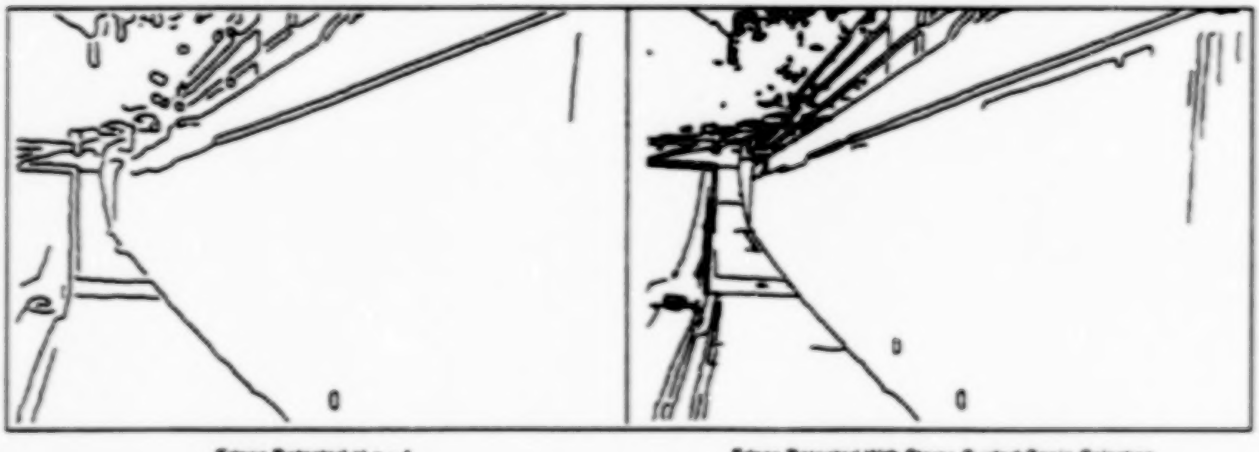

Edges Detected at $\sigma = 4$

Edges Detected With Stereo-Guided Scale Selection

Edges Were Detected by applying a gradient-based edge-detection algorithm to a Gaussian-filtered version of the original image. The edge-detection performance depends on the filter scale, σ.

A method of smoothing and edge detection in digitized images involves the use of a Gaussian smoothing filter that is adaptive in the sense that the filter scale varies with the estimated distance between each scene point and the camera. The estimate of distance is obtained via stereoscopy. The method was conceived for a developmental image-processing system that would recognize unexploded ordnance on a military test range. The method can also be used to enhance performance in other edge-detection applications.

Older methods of smoothing and edge detection involve, variously, the use of a sin-

gle scale or a set of scales, without knowledge of which scale is appropriate for each location in an image. In other words, the scale is not related to the sizes of objects in the image, even though the apparent sizes of objects vary widely with distance. As a result, the use of a single scale or an inappropriate set of scales for all image points can result in spurious edge detection or in failure to detect edges of interest.

In the present method, the scale at each point in an image is adjusted to account for the variation of apparent size with distance and is thus related to the real-world size of the object depicted at that point. The scale (σ) at pixel coordinates x,y is given by $\sigma(x,y) = K/R(x,y)$, where K is a predetermined constant and $R(x,y)$ is the distance computed at x,y from the disparity between the two images of a stereoscopic pair. The algorithm that computes $R(x,y)$ incorporates the calibration of the stereoscopic camera rig and includes a correction for radial lens distortion. The disparity between the left and right images for each pixel is obtained by minimizing the sum-of-squared-difference (SSD) measure of windows around the pixel in the Laplacian of the image. The coordinates of each pixel are then computed by triangulation. In the case of pixels for which $R(x,y)$ cannot be computed (e.g., where image texture is too low), $R(x,y)$ values are propagated from neighboring pixels by use of a technique that approximates nearest-neighbor search.

The variable-scale Gaussian smoothing filter is applied in a window of $2W+1$ by $2W+1$ pixels centered at the pixel x,y. Ideally, the output of the filter would be given by

$$S(x,y) = \sum_{i=-W}^{W} \sum_{j=-W}^{W} I(x+i, y+j) \frac{1}{\sigma(x,y)\sqrt{2\pi}} e^{-\frac{(i^2+j^2)}{2\sigma(x,y)^2}}$$

where $I(x,y)$ is the brightness of the image at x,y. It turns out to be inefficient to perform this computation exactly, using $\sigma = \sigma(x,y)$ for each pixel. For greater efficiency, the filter output is approximated by first convolving the entire image with a discrete set of Gaussian filters with scales related by factors of 2, then performing a parabolic interpolation to the appropriate scale for each pixel.

Edges are detected by an algorithm that computes gradients in the filtered image. For the purpose of edge detection, gradients must be comparable. However, gradients representing otherwise identical edges are stronger in regions smoothed at smaller values of σ. Therefore, to make gradients comparable, the magnitude of the gradient each pixel x,y is normalized by multiplying it by $\sigma(x,y)$.

The figure shows an original 750-by-500-pixel image along with examples of edge detection, without and with stereo-guided scale selection. At σ=1, edges close to the camera are rough and a number of extraneous edges are detected. As the scale jumps from σ=1 to σ=2 and σ=4, details of most distant objects (the trees and the far end of the railing) are lost. In the case of stereo-guided scale selection, edge-detection performance is high at both close and distant points in the scene.

This work was done by Clark F. Olson of Caltech for **NASA's Jet Propulsion Laboratory**. *Further information is contained in a TSP [see page 1].*
NPO-20475

Books and Reports

Development of Flight Software for Small Explorer Spacecraft

A report describes a continuing program of development of flight software for the attitude-control system (ACS) and the command-and-data-handling (C&DH) system of a prototype standard spacecraft of the Small Explorer (SMEX)-Lite class. Both the C&DH and ACS parts of the software are designed to run on a single reduced-instruction-set computer (RISC) with a peripheral component interface (PCI) bus architecture. The software consists of VxWorks tasks written in C++. Various components of the software have either been developed anew or redesigned from heritage code written for prior spacecraft missions. The development follows a "plug-n-play" approach — more specifically, an approach of object-oriented design and object-oriented programming, according to which the component of flight software corresponding to a particular sensor or actuator is treated as an object. This approach greatly reduces the time and risk of writing software to satisfy the distinct requirements for each of a wide range of SMEX-Lite missions. Another benefit of this approach is that the effort of testing spacecraft systems becomes focused on testing new functions and capabilities only, instead of retesting the entire spacecraft flight software system.

This work was done by Stephan R. Hammers of the Hammers Co. for **Goddard Space Flight Center**. *To obtain a copy of the report, "SMEX-Lite ACS and C&DH Flight Software," see TSP's [page 1].*
GSC-14214

END

01-28-00